Lawrence Berkeley National Laboratory
Recent Work

Title

Tracer Transport in Fractures: Analysis of Field Data Based on a Variable-Aperture Channel Model

Permalink

https://escholarship.org/uc/item/3hn6w17z

Journal

Water Resources Research, 27(12)

Authors

Tsang, Chin-Fu
Tsang, Y.W.
Hale, F.V.

Publication Date

1990-08-01

eScholarship.org Powered by the California Digital Library
University of California

UC 403
LBL-29474
Preprint

Lawrence Berkeley Laboratory
UNIVERSITY OF CALIFORNIA

EARTH SCIENCES DIVISION

Submitted to Water Resources Research

Tracer Transport in Fractures: Analysis of Field Data Based on a Variable-Aperture Channel Model

C.F. Tsang, Y.W. Tsang, and F.V. Hale

August 1990

For Reference

Not to be taken from this room

Prepared for the U.S. Department of Energy under Contract Number DE-AC03-76SF00098.

Copy 1
Bldg. 50 Library.

LBL-29474

DISCLAIMER

This document was prepared as an account of work sponsored by the United States Government. While this document is believed to contain correct information, neither the United States Government nor any agency thereof, nor the Regents of the University of California, nor any of their employees, makes any warranty, express or implied, or assumes any legal responsibility for the accuracy, completeness, or usefulness of any information, apparatus, product, or process disclosed, or represents that its use would not infringe privately owned rights. Reference herein to any specific commercial product, process, or service by its trade name, trademark, manufacturer, or otherwise, does not necessarily constitute or imply its endorsement, recommendation, or favoring by the United States Government or any agency thereof, or the Regents of the University of California. The views and opinions of authors expressed herein do not necessarily state or reflect those of the United States Government or any agency thereof or the Regents of the University of California.

LBL-29474

Tracer Transport in Fractures: Analysis of Field Data Based on a Variable-Aperture Channel Model

C. F. Tsang, Y. W. Tsang, and F. V. Hale

Earth Sciences Division
Lawrence Berkeley Laboratory
University of California
Berkeley, California 94720

August 1990

Submitted to *Water Resources Research*

This work was supported jointly by the Director, Office of Energy Research, Office of Basic Energy Sciences, Engineering and Geosciences Division, and by the Director, Office of Civilian Radioactive Waste Management, Office of Facilities Siting and Development, Siting and Facilities Technology Division, of the U.S. Department of Energy under Contract No. DE-AC03-76SF00098.

Tracer Transport in Fractures: Analysis of Field Data Based on a Variable-Aperture Channel Model

C.F. Tsang, Y.W. Tsang and F.V. Hale

Earth Sciences Division
Lawrence Berkeley Laboratory
University of California
Berkeley, California 94720

ABSTRACT

A variable-aperture channel model is used as the basis to interpret data from a three-year tracer transport experiment in fractured rocks. The data come from the so-called Stripa-3D experiment performed by Neretnieks and coworkers. Within the framework of the variable-aperture channel conceptual model, tracers are envisioned as travelling along a number of variable-aperture flow channels, whose properties are related to the mean $\bar{b}$ and standard deviation σ_b of the fracture aperture distribution. Two methods are developed to address the presence of strong time variation of the tracer injection flow rate in this experiment. The first approximates the early part of the injection history by an exponential decay function and is applicable to the early time tracer breakthrough data. The second is a deconvolution method involving the use of Toeplitz matrices and is applicable over the complete period of variable injection of the tracers. Both methods give consistent results. These results include not only estimates of $\bar{b}$ and σ, but also ranges of Peclet numbers, dispersivity and an estimate of the number of channels involved in the tracer transport. An interesting and surprising observation is that the data indicate that the Peclet number increases with the mean travel time; i.e., dispersivity decreasing with mean travel time. This trend is consistent with calculated results of tracer transport in multiple variable-aperture fractures in series. The meaning of this trend is discussed in terms of the strong heterogeneity of the flow system.

INTRODUCTION

Tracer transport in fractured media is quite different from that in porous media. The latter is often studied as a homogeneous three-dimensional (3D) flow and transport problem. For the former, on the other hand, if the matrix permeability is negligibly small compared to the fracture permeability, the flow and transport are in two-dimensional (2D) planes (representing fractures) in a highly heterogeneous three-dimensional space. A representative elementary volume may be defined for a homogeneous porous medium, but for fracture systems a representative elementary volume usually cannot be defined. Furthermore, recent experimental studies (Abelin et al., 1985, 1987; Bourke, 1987) have demonstrated that channeling effects occur in flow in the fracture plane. Thus the whole fracture plane is not uniformly conductive to water, but majority of flow occurs in flow paths of least resistance (or channels). With all these special features, tracer transport in fracture systems is a subject of active research, both experimental and theoretical.

One of the most comprehensive, multi-year tracer transport experiments in fractured rocks was performed by Neretnieks and co-workers (Neretnieks, 1987; Abelin et al., 1987) in the Stripa Mine in Sweden over the years 1984–1987. The experiment, commonly referred to as the Stripa-3D Experiment, unveiled a number of interesting and important characteristics of flow and transport in fractured systems. In this paper we are mainly concerned with the analysis of these tracer data.

Since the conventional three-dimensional homogeneous porous model is not an appropriate representation of the fracture system, a new theoretical approach has to be adopted as a basis for the analysis of Stripa-3D data. A number of approaches for transport in fractured media have been proposed in the literature (Endo et al., 1984; Robin-

son, 1984; Schwartz and Smith, 1988). In this paper we extend and apply a variable-aperture channel model (Tsang and Tsang, 1987; Tsang et al., 1988; Tsang and Tsang, 1989) as the basis for the analysis of the Stripa-3D data.

In the experiment, due to various constraints, the tracer injection flow rates are strongly fluctuating. We developed two analytic methods to take this into account. The first method, representing a preliminary and crude analysis, considers only the early time portion of the data where the injection can be approximated by an exponential decay function, followed by a constant rate. An analytic solution to such a case is fitted to the early part of the tracer breakthrough curves to obtain estimates for both the dispersion coefficient and the mean transport velocity. The second method applies a deconvolution procedure to the variable injection flow rate and the corresponding tracer breakthrough curves to obtain the equivalent breakthrough curves for a delta function pulse injection. Both analytic methods will be developed below.

The purpose of the paper is three-fold. First, we would like to study the usefulness of the recently developed variable-aperture channel conceptual model for the analysis of transport data in fractures. Second, we develop the necessary analytic tools and computer codes for such an analysis. Third, we obtain estimates for the parameters which characterize transport in the Stripa system of fractures.

A SUMMARY OF STRIPA-3D EXPERIMENT

Details of the Stripa-3D experiment are given by Neretnieks (1987) and Abelin, et al. (1987). The experiment was carried out in the Stripa mine in two drifts in the form of a cross, as shown in Figure 1a. The longer drift is 75 m long and the shorter intersecting drift is 25 m long. Each drift is 4.5 m in width and 3 m in maximum height. Three

vertical boreholes are drilled into the ceilings of the drifts; and in these boreholes nine packered off sections (1 m long) were identified as having large enough local hydraulic conductivity to be suitable for tracer injection. Nine tracers were used and were distributed among the three boreholes as shown in Figure 1b. These tracers were collected in over 300 plastic sheets of 1×2 m each, covering the ceiling and sides of the drifts. The flow rates at the collection plastic sheets are approximately constant in time, indicating that steady state flow conditions prevail. However, the majority of these sheets did not receive significant flow, and tracer mass tended to concentrate at discrete regions of the drift (see Figures 2a and 2b).

Only five of the nine tracers are found in significant concentrations in the different plastic collection sheets during the first 30 months of the experiment. These were eosin B, eosin Y, uranine, elbenyl and iodine. The apparent linear transport distances ranged from 10 m to 45 m. Figure 3 shows the injection flow rates as a function of time. The tracer breakthrough into the sheets is localized to a small number of sheets around the X location of 24 to 36 m, where X is measured along the axis of the longer drift. This is illustrated in Figures 4a and 4b, where the tracer mass return rate over all the sheets as a function of time is plotted and compared with the tracer mass return rate over only the sheets between X = 24 to 36 m. It is apparent that nearly all the tracer mass is colleced in this limited section.

A SUMMARY OF THE VARIABLE-APERTURE CHANNEL MODEL

The concept of flow channels was introduced to the study of fractured rocks by Neretnieks and coworkers (Neretnieks, 1983, 1987; Abelin et al., 1985) based on their experiments in single and multiple fractures in Stripa. Motivated by this, Tsang and

Tsang (1987) developed the model in which transport through fractured rocks is controlled by a number of channels, each of which has variable apertures along its length. These variable apertures define an aperture probability distribution function which describes the aperture distribution over the two-dimensional plane of a single fracture. Later, Tsang and Tsang (1989) pointed out that these channels are not physical pipes in the fracture plane, but that they arise directly from the wide range of apertures distributed over each fracture. Figure 5 shows schematically a square section of fracture with a spatial distribution of apertures (Fig. 5a) and the flow channeling that results by imposing a potential difference from left to right (Fig. 5b). In Figure 5b, the thickness of lines is made arbitrarily proportional to the square root of the flow rate along the flow path. Thus flow channeling is manifested by the occurrence of a few tortuous channels, each of which is composed of a number of flow paths of comparable mean velocities.

Flow and transport through a system of fractures can then be envisioned as occurring through these tortuous channels of flow paths from fracture to fracture in the three-dimensional space (Fig. 6). These channels may intersect each other within a fracture plane and also between fractures when fractures intersect in a fracture network. The hydraulic conductivity of each channel is controlled by constrictions along the channel, and which is therefore not directly related to the volume or average aperture value of the channel. Transport in the system is then hypothesized to be dependent on the aperture probability density distribution with a mean aperture value $\bar{b}$ and a spread or standard deviation σ_b, and on the spatial arrangement of the apertures characterized by the spatial correlation length λ.

In many tracer transport experiments the measuring scale is such that the transport distances cover only a few fracture spacings in a fracture network, in which case transport can be studied as flow through a number of fractures in series. A large number of fractures may be generated by a geostatistical method with a specified aperture probability density distribution and a spatial correlation length, and the local flow rates in each of these fractures may be solved separately following our earlier model (Moreno et al. 1988). Then the fracture may be put in series, satisfying the continuity requirement that the identical total flow rate must occur in each fracture. Particle tracking is then carried out in the series of fractures. This conceptualization of fracture-in-series calculations requires the intersection between two fractures to be an equipotential line, which is a reasonable approximation based on the common observation in mines and drifts that the most conductive zone often occurs at intersection of fractures (Abelin et al., 1987). We have carried out calculations for two, three, four, and up to 100 fractures in series. The larger numbers of fractures are of theoretical interest only, since for that many fractures the 3D fracture network effect starts to dominate, and thereby invalidating the fracture in series approximation.

The flow results for two fractures in series are shown in Fig. 7, where the channeling from fracture to fracture is clearly shown. Now let us introduce tracer particles on the left side of the series of fractures and measure tracer breakthrough on the right. If observation is over only a small window on the right-hand edge of the fractures, the observed tracer breakthrough will depend sensitively on the window location, with the maximum concentration ranging from zero to a large amount and with very different dispersion characteristics. However, if the observation window is larger, or in other words, a spatial average is taken over a tracer emergence line or surface, the variation of

the dispersion properties is reduced drastically (Tsang, 1989). It was demonstrated that this averaging should be over two or three spatial correlation lengths λ. The dispersion value of such averaged tracer breakthrough may then be related to fracture aperture parameters $\bar{b}$ and σ_b (Tsang et al., 1988). In data analysis discussed below, the spatial averaging is done by summing the products of the concentration of a particular tracer and the instanteous flow rate at each collection sheet, and then dividing by the sum of flow rates from all the contributing collection sheets. In this way, we arrive at one breakthrough curve for each tracer, averaged over the collection sheets, as shown in Figure 4.

For a breakthrough curve where the concentration is plotted against time, the quantity $(t(0.9) - t(0.1))/t(0.5)$ is a measure of the dispersion, where t(p) denoting the time when a fraction, p, of the maximum tracer concentration arrives at the exit line. An interesting result for the calculated dispersion in the breakthrough for a system of fractures in series is shown in Figure 8 where we plot the value of $(t(0.9) - t(0.1))/t(0.5)$ versus the number of fractures in series traversed by the tracer. A decrease of this dispersion measure is found with travel distance and hence, travel time. One possible physical explanation for this trend is as follows. Before the 3D network effect becomes important the characteristic dispersive length depends only on σ_b and λ. These parameters characterize the fracture apertures in a single fracture and are assumed to be applicable to all the fractures in series. The dispersion of advective transport is then a measure of the different possible paths a tracer particle can take in traveling from the injection to the observation locations, and an increase in travel distance implies that each of these paths would sample a better statistical average of the variations. Thus travel times along these paths become more and more similar and a decrease of dispersion with travel distance is expected. This holds true only when tracer transport distance is less than a certain

number of fracture spacings in the fracture network, prior to the setting in of 3D network effect, at which point we woud expect the measure of dispersion to increase again. The number of fractures for which the fracture in series picture is applicable is not yet well established and a Monte Carlo calculation is underway to define it. Our preliminary results show that the number may be of the order of 5 to 8, depending on the ratio of fracture size to fracture spacing.

DATA ANALYSIS METHODS

We proceed to study and analyze the Stripa-3D data based on the insight gained from the variable-aperture channel model. The model suggests that we can consider the tracers to travel along several tortuous channels in a three-dimensional space, each of which is composed of a number of flow paths of comparable but not identical mean velocities, thus giving rise to some kind of dispersion within the 'flow channel'. Of the flow paths which make up the channel, each flow path has variable apertures along its length. No dispersion (Taylor dispersion) is considered within each flow path, and we have ignored possible matrix diffusion and chemical retardation processes with the implicit assumption that the tracers used are conservative over the relatively small travel times (as compared with the time frame of matrix diffusion and chemical retardation processes), so that these are not significant factors. Furthermore, we assume that the travel distances cover only a few fracture spacings so that the 3D fracture network effects are not important. Under all these assumptions, flow velocities and dispersion measures of these 1D channels will be obtained and will be shown to be related to each other and to the basic fracture parameters $\bar{b}$ and σ_b, characterizing the variable-aperture channel model.

Our conceptual model of the Stripa-3D experiment is as follows. Because the underground drift is maintained at atmospheric pressure, it is a major sink for water from the rock around it. The large range of aperture values in the fractures gives rise to flow channeling so that the majority of flow takes place in only selected flow paths of least flow resistance which comprise only a small fraction of the total 3D flow region. When a tracer is injected at a particular location in the flow field, the resultant solution moves downstream along these preferred flow paths toward the drift and emerges in a number of plastic collection sheets. From the experimental measurements we do not have knowledge of the actual flow paths connecting the tracer injection and the particular collection sheet of tracer emergence. However, from the time dependence of the tracer collection, it will be shown below that we can identify channels or groups of flow paths which have comparable residence times.

At Stripa, dilution of the injected tracers is clearly present because the tracer injection flow rate q is much smaller than the total exit flow rates at the drift, and also, while the injection flow rate is strongly varying, the collection flow rate is fairly constant over time. Because of the unknown dilution effect of the channel flow, the absolute value of the concentration of the breakthrough curves will not be investigated, and actually this is not needed to obtain the relevant parameters such as mean and standard deviation of aperture values along the flow paths which govern and characterize the advective transport in the fractured medium. In our analysis below, we used the rate of tracer mass accumulation as the observed quantity rather than the more commonly used tracer concentration.

Thus in this conceptual picture, one has a flow channel with emerging flow rate Q at the collection location while tracer is injected with a given mass per unit time at an upstream location. The tracer mass injected per unit time is proportional to injection flow rate q if the injected tracer concentration is constant, as is the case in this experiment. Assuming that the one-dimensional advective-diffusive transport equation holds in the 1D channels, well known analytic solutions are available for the analysis of tracer transport data. The main complication with the present data set is the strong temporal variation of the tracer injection flow rate (Figure 3). Two approaches are developed to address this, which are described in the next two subsections.

Analysis of First Peak Early Arrival Data

The injection flow rate data (Figure 3) vary strongly with time, but all of the early time data display a sharp decline which may be closely approximated by an exponential decay and then a period of stabilization (see Figure 9). As a preliminary analysis of Stripa 3D field data, we study this early part of injection data and the corresponding early part of the tracer breakthrough curves. The early time injection input may be written as:

$$\frac{C_i(t)}{C_o} = \frac{q(t)}{q_o}$$

$$= e^{-\alpha t} \qquad t < t_o$$

$$= \text{constant} = e^{-\alpha t_o} \qquad t \geq t_o \ , \tag{1}$$

where C_i is the concentration of injected solute at the injection point and $C_o = C_i(t=0)$. The time t_o is chosen to be the time at which the injection flow rate is near the first major minimum. Then the parameter α is obtained by fitting the area under the curve $q(t)/q_o$ to that of field data over the interval $t = 0, t_o$. Sensitivity studies show that the analysis

results are not sensitive to the exact values of t_o chosen so long as t_o is larger than the time at first minimum and the early drop of $q(t)/q_o$ values is reasonably reproduced. An analytic solution of the advective-diffusive equation for the injection rate given by Eq. (1) is available (see, e.g., Javandel et al., 1984); it is

$$C(x,t) = C_o e^{-\alpha t} A_1(x,t) \qquad 0 < t \le t_o$$

$$C(x,t) = C_o \left[e^{-\alpha t} A_1(x,t) - e^{-\alpha t} A_1(x,t-t_o) + e^{-\alpha t_o} A_2(x,t-t_o) \right] \text{ for } t_o < t \qquad (2)$$

where

$$A_1(x,t) = \left[\frac{v}{v+U} \right] e^{\frac{x(v-U)}{2D}} \operatorname{erfc}\left[\frac{x-Ut}{\sqrt{4Dt}} \right] +$$

$$+ \left[\frac{v}{v-U} \right] e^{\frac{x(v+U)}{2D}} \operatorname{erfc}\left[\frac{x+Ut}{\sqrt{4Dt}} \right] -$$

$$- \left[\frac{v^2}{2D\alpha} \right] e^{\left[\frac{vx}{D} + \alpha t \right]}$$

$$A_2(x,t) = \tfrac{1}{2} \operatorname{erfc}\left[\frac{x-vt}{\sqrt{4Dt}} \right] + \sqrt{\frac{v^2 t}{\pi D}}\, e^{-\frac{(x-vt)^2}{4Dt}} -$$

$$- \tfrac{1}{2} \left[1 + \frac{vx}{D} + \frac{v^2 t}{D} \right] e^{\frac{vx}{D}} \operatorname{erfc}\left[\frac{x+vt}{\sqrt{4Dt}} \right],$$

and

$$U = \sqrt{v^2 - 4D\alpha}\ .$$

The solution has two parameters: the mean flow velocity in the channel v, and the channel longitudinal dispersion coeffcient D arising from the slightly different velocities of the various flow paths that comprise the channel. Figure 10 displays this solution for a fixed value of v = .01 m/hr and as a function of D which ranged from 10^{-4} to 1 m^2/hr. The range of values used for D yields either real or imaginary values for U, but they all

result in real values for A_1. The calculational procedure involves the realization that equation (2) contains terms of the form e^a . erfc(b), where a and b are complex numbers. For certain values of parameters the complex complementary error function in this term can take on very small values while the exponential function very large values. Hence the evaluation of this term is carried out by regrouping the factors:

$$e^a \cdot \mathrm{erfc}(b) = e^{a-b^2}\, w(ib),$$

where

$$w(ib) = e^{b^2}\, \mathrm{erfc}(b).$$

The function w(z) may be evaluated either with a library subroutine or a continued fraction approximation. Figure 10 shows the special case that $C_i/C_o = 0$ for $t > t_o$. The broadening of the breakthrough curves with increasing long tail as the value of D increases is clearly displayed. The longitudinal dispersion coefficient D controls the shape (or spread) of the early part of the breakthrough curves, while the mean tracer transport velocity v determines the arrival time of the first concentration peak in the breakthrough curve. These two parameters are adjusted to match the early-time data of the measured tracer arrival breakthrough curves by an iterative process using initial guess values. The early time data used for fitting covers the data points up to the first peak. A typical fit is shown in Figure 11. The results for the five tracers are given in Table 1, which also shows the apparent linear distance X from injection point to the weighted center of exit locations in the drift ceiling, and the arrival time of the first peak t_p.

From the fitted D and v values obtained one may calculate the mean arrival time, $\bar{t}$, corresponding to a delta pulse injection at time t = 0, where $\bar{t}$ is given by (see e.g., Robinson, 1984)

$$\bar{t} = \frac{x}{v} + \frac{D}{v^2} .$$

The dispersivity α and Peclet number Pe are calculated according to the formulae

$$\alpha = D/v$$

and

$$Pe = vx/D,$$

and they are listed in Table 1. The dispersivity values from the five tracer injection tests range from 1.8 to 6.8 m, and the corresponding Pe values, from 3.0 to 24. A further discussion of these results will be given later.

Toeplitz Analysis of Tracer Data

To analyze the full time range of tracer breakthrough data for the variable injection flow rate, we resort to a deconvolution method similar to that used in signal processing and information theories and to the unit hydrograph method of surface hydrology (Eagleson et al., 1966; Dreiss, 1982; Neuman and de Marsily, 1976). We have developed a simplified formulation which is particularly suited to discretized data. The method, given below, assumes that the system response is linear and that it is stable with time.

Let the variable tracer incremental injection mass flow rate m_j be discretized so that $m_j = (qC_i)_j$, where j is the index for successive times and q is the temporally variable tracer input flow rate (L^3/T) and C_i is the constant input concentration (dimension M/L^3). Let M_i be the discretized incremental tracer mass breakthrough at the observation location, where i is again the index for successive times. For each input element m_j at time t_j, we may define a unit response function a_{ij} which gives the observed breakthrough $(QC)_i = M_i$ at time t_i. In general, for each j, there is a range of i values for which a_{ij} is nonzero. Since the response function should be invariant to time translation ($i \rightarrow i + n$

and $j \rightarrow j + n$), a_{ij} should only be a function of $t_i - t_j$, i.e., $a_{ij} = a_{i-j}$. Hence the matrix a_{ij} may be completely defined by a column vector a_{i-j}. Furthermore, the response time i, should always be later than input time j due to causality, so that $a_{ij} = 0$ if $i \leq j$. Then for all the input elements m_j, the output M_i is given by the superposition:

$$M_i = \sum_j a_{ij} m_j \tag{3}$$

where

$$a_{ij} = a_{i+n,j+n}$$

and

$$a_{ij} = 0 \quad \text{if} \quad i < j \ .$$

The a_{ij} defined this way is the Toeplitz matrix (Gohberg, 1982; Gray, 1977), which has the interesting property that it can be completely defined by a column vector. It can be shown that equation (3) may be rewritten with the response of the system, a, represented by a vector, and the injection rate, m, represented as a Toeplitz matrix:

$$a_{ij} = a_s \ ; \quad s = i-j$$

$$m_j = m_{is} \ ; \quad j = i-s$$

and

$$M_i = \sum_s m_{is} a_s \tag{4}$$

In matrix form, this equation may be denoted by

$$\underline{M} = \underline{\underline{m}} \cdot \underline{a} \tag{5}$$

so that

$$\underline{a} = \underline{\underline{m}}^{-1} \underline{M} \tag{6}$$

The vector $\underline{a}$ is the unit response function or tracer breakthrough curve (whose elements are a_j with index j denoting the time sequence) due to a unit delta function pulse tracer

injection at t = 0. For a homogeneous 1D porous medium, the response a_j is simply the Green's function to an advective diffusive equation for the unit delta function source (see e. g. Kreft and Zuber, 1978):

$$a_j = \frac{R}{\sqrt{4\pi D t_j}} e^{-\frac{(x - vt_j)^2}{4Dt_j}}, \tag{7}$$

where R is a constant proportional to the initial mass injected per unit channel cross-section area at the input location. For a fractured medium with flow channeling, the reponse a_j will display multiple peaks as illustrated in Figure 12. Each of these peaks can be described by Equation (7).

In principle, given the input tracer injection variable function and the measured tracer breakthrough curves, they can be discretized into time-stepped values to form the column vectors $\underline{m}$ and $\underline{M}$ respectively. Then the Toeplitz matrix $\underline{\underline{m}}$ can be formed from the vector $\underline{m}$ by setting $m_{ij} = m_s$, where $s = i-j$. Then equation (6) can be solved for $\underline{a}$ directly and exactly.

In practice, however, both $\underline{m}$ and $\underline{M}$ contain measurement errors, and these errors may easily multiply in the solution for $\underline{a}$, and negative values of a_i are sometimes obtained. To ensure that a_i are positive, as they should be on physical grounds, and to reduce the influence of errors, we go back to equation (4) and employ a least square fit method.

$$f(a_s) = \sum_{i=1}^{N} \left[M_i - \sum_{s=1}^{i} (a_s)\, m_{is} \right]^2 \tag{8}$$

where a_s may be adjusted within the positive-value domain to minimize the function $f(a_s)$. As a further practical step, if the first of tracer arrival time is denoted by the index s_o, we can set all $a_s = 0$ where $s < s_o$ and take them out of the fitting and minimization

process.

We have applied the above procedure to the five sets of tracer data under study. Data were digitized to averaging steps of 500 hours. We have also used averaging steps of 1000 hours in a sensitivity study which shows little effect on the final solution. In this procedure, equation (6) is first solved to obtain an initial set of guess solutions for a_s, and any negative a_s values obtained are arbitrarily set to a very small positive value. The equation (9) is then minimized with the condition that a_s must be positive. Stable unique solutions for a_s were found in all cases. The results of the deconvolution procedures are shown in Figures 13 to 17, with the circles denoting the derived response of the fractured medium to a unit delta function pulse injection.

To test the stability of these solutions to errors in breakthrough data, non-systematic random errors were introduced into the discretized data up to 20% of their value. Figure 28 shows the results of the study, where a_j obtained from 50 realizations of these data sets with randomized errors are shown. Very similar results in a_j were obtained.

The data a_j in Figures 13 to 17 clearly unveil the multiple channel nature of the tracer transport in the Stripa-3D data. Over the range of distances and observation time periods, eosin-B apparently has four major channels, while the other tracers have two channels each. Note that we have defined a channel as a group of nearby flow paths with comparable mean velocities. These results were obtained by applying the Toeplitz analysis to the mean concentration breakthrough curves averaged over all the collection sheets where the tracer arrived. The same analysis was also applied to tracer breakthrough curves for a few specific collection sheets at a single X distance along the experimental drift. The same patterns as those shown in Figures 13–17 are obtained. In other

words, take the example of eosin B, the four-channel pattern shown in Figure 13 is also found if one applies Toeplitz analysis to only sheets at X = 27 or only to those at X = 43 m. Thus the channels do not correspond to different flow tubes arriving at different collection sheets, but rather all sheets appear to display the same multi-channel structure in their respective tracer breakthrough curves.

To quantitatively characterize the channels, we fit the solution of the 1D advective diffusive equation with a delta function tracer injection, given by equation (7), to each of these peaks in Figures 13 to 17. That is, the data in these figures are fitted to

$$a_j = \sum_n \frac{R_n}{\sqrt{4\pi D_n t_j}} e^{\frac{-(x - v_n t_j)^2}{4 D_n t_j}} \tag{9}$$

where we have allowed v and D in Eq. (7) to be different for different channels and denoted them with the subscript n. Thus v and D for each channel are obtained, and a Peclet number is derived for each channel as before. The results are tabulated in Table 2. The results point out (1) indeed the variable-aperture channel model seems to be confirmed by the Stripa-3D data, with travel distances from 10–43 m and mean travel times from 2600 to 16000 hours; (2) the number of channels involved in tracer transport at this site under conditions of this set of experiments ranges from two to four, (3) dispersivity values range from very small to 2.9 m.

DISCUSSION

In the last section we showed that after deconvolution, the tracer breakthrough curves corresponding to delta function input display multiple peaks. We calculated the Peclet number corresponding to each peak. This is in contrast to the usual practice which involves the calculation of Peclet number and dispersion for the tracer breakthrough

curve in its entirety for a delta function tracer injection. In that case the Peclet number would be much smaller and dispersion larger. In the discussion of Peclet number below it is to be emphasized that we do not refer to the Peclet number in the usual sense, but to the Peclet number for each channeled transport within the framework of the channel model. In examining Table 1 and Table 2, we do not find a clear simple dependence of Pe number with the apparent linear travel distance over the range studied. However, if we plot Pe against the mean travel time from results obtained by both methods of analysis we find an interesting behavior. Figure 19 shows Pe values versus mean arrival time in a log-log plot. In this figure we see that points for results from the Toeplitz analysis and from the first peak initial data analysis display the same trend. Consistency of results from these two rather different methods provides some confidence on the validity of this trend. Thus there appears to be a general increase of Pe number as a function of mean travel time, implying a decrease of dispersion with travel time. This is in qualitative agreement with the multi-fracture modeling study results (Figure 8) discussed in an earlier section. Furthermore, in the log-log plot (Figure 19) the points fall roughly between two straight lines with slopes of 1.7 and 2.7 respectively. Hence these results indicate a relationship between Pe number and mean travel time $\bar{t}$ as follows:

$$\log Pe = n \log \bar{t} + \text{constant}$$

so that

$$Pe \propto \bar{t}^{n}, \quad \text{where } n = 2.2 \pm 0.5$$

However we do not believe that the data are good enough to determine the n value to this degree of certainty. We could equally well state that

$Pe \approx \bar{t}^2$.

The values of $\alpha = x/Pe$ obtained for each individual channel are also displayed in Figures 20 as a function of mean travel time in a log-log plot. This figure shows that the Stripa-3D data appears to indicate $\alpha \approx (\bar{t})^{-2}$

The values of α calculated by the Toeplitz method (Table 2) range from 0.03 to 2.9 meters. However the values for the first channels (for early times) for all the tracers, which may be subject to less analysis error than those of the later channels, range from 0.6 to 2.9 m. These are consistent with those from the first peak initial data analysis.

The surprising result that $Pe \approx \bar{t}^2$ or $\alpha \approx 1/\bar{t}^2$ is a direct result of the analysis of the field data. It is in contrast to the case of a porous medium where the Peclet number is usually assumed to be constant with respect to mean travel time $\bar{t}$. It is also different from the result for flow in a constant-diameter pipe, where the time dependence is given by the Taylor's dispersion, which for small molecular dispersion gives $Pe \approx \bar{t}$. In Stripa 3D data, we find a much stronger $\bar{t}$ dependence for transport through variable-aperture fractures. The basis and implication of this interesting result are yet to be studied. One possible explanation is as follows. Consider the results of deconvolution for all five sets of data shown in Figures 13-17. It can be seen that the standard deviation σ_t of tracer particle arrival times for each of the peaks is about the same with the other peaks in each case, i.e., σ_t appears to be independent of the mean travel times of the peaks. Since the Peclet number for 1D transport along a channel may be expressed (Levenspiel, 1972) as:

$$Pe = 2\frac{\bar{t}^2}{\sigma_t^2}$$

then $Pe \approx \bar{t}^2$. Now, σ_t is dependent on the variance of fracture apertures or local per-

meabilities over the 2D fracture plane. For tracer transport along different channels between injection and collection points, this may be approximately the same, since the tortuocity is not expected to affect the real travel path length by more than a factor of two or so. However, the mean travel times of these channels may be strongly affected by the local heterogeneity. Thus a local constriction or a relatively large local aperture volume along a flow channel will strongly affect the mean travel times. In other words, for a strongly 2D heterogeneous system as in our case, the mean travel time and the travel time standard deviation may be decoupled. If we extrapolate this line of reasoning, we may conjecture that for the type of system under study, we should not focus on the Peclet number or the dispersivity. Rather, we should determine the travel time standard deviations σ_t and mean travel times $\bar{t}$ of the groups of flow paths, or channels. The former, σ_t, is closely correlated to aperture or permeability variance, and can be estimated for the case of Stripa-3D data discussed above. The latter, $\bar{t}$, is strongly affected by the local heterogeneity around the injection location and has not been correlated to aperture distribution parameters in our case study. However, if one is able to study the $\bar{t}$ values for a larger number of such transport channels, we expect that the mean of these $\bar{t}$ values can be correlated to the basic aperture probability distribution parameters.

The mean apertures $\bar{b}$ of the flow channels responsible for transport may be estimated from the experimental flow rates Q to the 1×2 m tracer collection sheets and the calculated velocities v from the first peaks or first channels in Table 1 or 2. At a collection sheet on the drift ceiling, the observed incoming flow rate is fed by flows with different tracers with velocities v_i. If the average channel width covered by the collection sheet is w and the mean fracture aperture is $\bar{b}$, then

$$Q = \sum_i \bar{b}\, w\, v_i = \bar{b}\, w \sum_i v_i = A \sum_i v_i ,$$

where A is the cross-sectional area of the conducting fractures in the collection sheet and $\sum_i v_i$ is the sum of velocities of tracers that arrive at the sheet. From Abelin et al. (1987), the averaged inflow rate Q is about 20 ml/hr for those sheets with large flow rates (distance along the drift X = 24-36 m). The average width of the flow channels, w, is not determined within the present data set. For sheets in region X = 24 - 36m where there were large flow rates, we assumed that the relevant width w = 1m is a reasonable estimate. Then from Table 1, $\sum_i v_i$ for all 5 tracers is 59 mm/hr. Combining all numbers, we find $A = Q/\sum_i v_i = 0.3 \times 10^{-3}$ m^2 and $\bar{b} = A/w = 300$ μm. If we use just the first channel velocities from Table 2, $\sum_i v_i = 38$ mm/hr and we obtain $A = 0.5 \times 10^{-3}$ m^2 and $\bar{b} = 500$ μm. The calculations were also made for each sheet independently. Some of the detailed results were shown in Table 3.

Another quantity that we can estimate from these results is σ_b, the standard deviation of the aperture distribution function. For this, we follow the procedure presented in Tsang et al. (1988). Starting with the Pe numbers for the first peak or first channels given in Tables 1 and 2, and assuming that the channel flow obeys 1D advective dispersive equation (see e.g. Neretnieks et al., 1982), we find that the dispersion measure (t(0.9) – t(0.1))/t(0.5) ranges from 0.5 to 1.7. Tsang et al. (1988) give a graphical relationship between this dispersion measure and the aperture variance $s = \sigma_b/\bar{b}$. Applying that relationship, we obtain values of $\sigma_b/\bar{b}$ ranging from 0.35 to 0.75. Thus if $\bar{b} = 300$ μm, σ_b for the Stripa fracture system is estimated to be 105–225 μm.

Table 4 summarizes the major conclusions from both analysis methods on the Stripa-3D tracer data.

SUMMARY AND CONCLUSIONS

A fractured medium represents a strongly heterogeneous system. Tracer transport in such a medium cannot usually be understood by assuming flow and transport in a 3D homogeneous permeable system. In the Stripa-3D experiment the heterogeneity of the medium causes tracers to emerge at the experimental drift ceiling and walls in isolated spots. This kind of channelized flow path requires new approaches for its analysis. In this paper we applied the variable aperture channel model (Tsang and Tsang, 1987,1989; Tsang et al., 1988), which assumes that flow in a fractured medium is dominated by flow through a few variable-aperture channels, each of which is defined by a number of flow paths with comparable travel times. One may characterize the transport in each channel by a mean travel time and the dispersion coefficient. These parameters for the different channels are related to each other and to the basic parameters describing the fracture aperture distribution, $\bar{b}$ and σ_b.

This approach is applied to the analysis of the Stripa-3D data. Two analysis methods were developed and applied; (1) the first peak early arrival data analysis and (2) the Toeplitz analysis. The results led to a confirmation of the concept of multiple variable-aperture channels and to the determination of a number of parameter values that characterize the fractures. These parameters, summarized in Table 4, represent some of the important inputs that are needed for calculating travel times and dispersion characteristics of tracers traversing the medium. One surprising and interesting feature that emerges from these results is the time dependence of Peclet number or the apparent

dispersivity. It is qualitatively consistent with the results from the channel model for fractures in series with larger and larger travel distances and travel times, and may imply a time-independent σ_t for the particle arrival time in the flow channels. Further study, both experimental and theoretical, is needed to test this hypothesis and to understand its full significance.

ACKNOWLEDGMENTS

We have benefitted from the careful review and comments from G.S. Bodvarsson and C. Carnahan of Lawrence Berkeley Laboratory, Berkeley, California, and from L. Moreno and I. Neretnieks of the Royal Institute of Technology (KTH), Stockholm, Sweden. The paper was concluded during an extended visit of the first two authors to KTH in 1990. The hospitality and assistance of KTH staff, especially I. Neretnieks, L. Moreno and Margareta Lundberg are gratefully acknowledged. Work is jointly supported by the Director of Office of Energy Research, Office of Basic Energy Sciences, Engineering and Geosciences Division, and by the Director, Office of Civilian Radioactive Waste Management, Office of Facilities Siting and Development, Siting and Facilities Technology Division of the U. S. Department of Energy under contract No. DE-AC03-76SF00098.

REFERENCES

Abelin, H., Birgersson, L., Gidlund, J., Moreno, L., Neretnieks, I., Widen, H., and Agren, J., 1987. 3D migration experiment - report 3: performed experiments, results and evaluation. Stripa Project technical Report 87-21. Swedish Nuclear Fuel and Waste Management Company (SKB), Stockholm, Sweden, November 1987.

Abelin, H., Neretnieks, I., Tunbrant, S., and Moreno, L., 1985. Final report on the migration in a single fracture, Experimental results and evaluations, Svensk. Karnbransleforsorjning Tech. Report 85-03, Nucl. Fuel Safety Proj., Stockholm.

Bourke, P.J., 1987. Channeling of flow through fractures in rock, Proceedings of GEOVAL-87, International Symposium, Stockholm, Sweden, April 7–9, 1987.

Dreiss, S.J., 1982. Linear kernels for karst aquifers, Water Resour. Res., Vol. 18, No. 4, pp. 865–876.

Eagleson, P.S., Mejia-r, R., and March, F., 1966. Computation of optimum realizable unit hydrographs, Water Resour. Res., Vol. 2(4), pp. 755–764.

Endo, H.K., Long, J.C.S., Wilson, C.R., and Witherspoon, P.A., 1984. A model for investigating mechanical transport in fracture networks, Water Resour. Res., Vol. 20 (10), pp. 1390–1400.

Gohberg, I., 1982. Editor, Proceedings of Toeplitz Centennial: Toeplitz Memorial Conference in Operator Theory, Tel Aviv, May 11–15, 1981, Birkhaeuser Verlag, Basel.

Gray, R.M., 1977. Toeplitz and circulant matrices II, Information Systems Laboratory, Stanford Electronics Laboratory, Technical Report SEL 77-011, April, Stanford, Stanford, California.

Javandel, I., Doughty, C., and Tsang, C.F., 1984. Groundwater transport: Handbook of mathematical models, Water Resources Monograph 10, American Geophysical Union, Washington, D.C.

Kreft, A. and Zuber A., 1978. On the physical meaning of the dispersion equation and its solutions for different initial and boundary conditions, Chemical Engineering Science, Vol. 33, 1471-1480.

Levenspiel, O. 1972. Chemical reaction engineering, Second Edition, p. 275, John Wiley Publishers, New York.

Moreno, L., Tsang, Y.W., Tsang, C.F., Hale, F.V., and Neretnieks, I., 1988. Flow and tracer transport in a single fracture: A stochastic model and its relation to some field observations, Water Resour. Res., Vol. 24(12), pp. 2033–3048.

Neretnieks, I., 1983. A note on fracture flow dispersion mechanisms in the ground, Water Resour. Res., Vol. 19(2), pp. 364–370.

Neretnieks, I., 1987. Channeling effects in flow and transport in fractures rocks—some recent observations and models, Proceedings of GEOVAL-87, International Symposium, Stockholm, Sweden, April 7–9, 1987.

Neretnieks, I., Eriksen, T. and Tahtinen, P., 1982. Tracer movement in a single fissure in granitic rock: some experimental results and their interpretation, Water Resour. Res. Vol. 18 (4), pp.849-858.

Neuman, S.P., and de Marsily, G., 1976. Identification of linear systems response by parametric programming, Water Resour. Res., Vol. 12(2), pp. 253–262.

Robinson, P.C., 1984. Connectivity, flow and transport in network models of fractured media, Ph.D. thesis, Oxford University, London.

Schwartz, F.W., and Smith, L., 1988. A continuum approach for modeling mass transport in fractured media, Water Resour. Res., Vol. 24(8), pp. 1360–1372.

Tsang, C.F., 1989. Tracer travel time and model validation, International Journal of Radioactive Waste Management and the Nuclear Fuel Cycle, Vol. 13(1-4), pp. 311–323.

Tsang, Y.W., and Tsang, C.F., 1987. Channel model of flow through fractured media, Water Resour. Res., Vol. 23(3), pp. 467–479.

Tsang, Y.W., and Tsang, C.F., 1989. Flow channeling in a single fracture as a two-dimensional strongly heterogeneous permeable medium, Water Resour. Res., Vol. 25(9), pp. 2076–2080.

Tsang, Y.W., Tsang, C.F., Neretnieks, I., and Moreno, L., 1988. Flow and tracer transport in fractured media—A variable aperture channel model and its properties, Water Resources Research, Vol. 24, no. 12, pp. 2049–2060.

Table 1. Results of Analysis of First Peak Early Time Data

Tracer	x (m)	t_p (hr)	D (m·mm/hr)	v (mm/hr)	x/t_p (mm/hr)	$\bar{t}=\frac{x}{v}+\frac{D}{v^2}$ (hr)	$\alpha=D/v$ (m)	Pec =vx/D
Elbenyl	10.7	2500	14.	3.8	4.3	3700	3.6	3.0
Eosin Y	24.6	8500	7.5	3.2	2.9	8300	2.3	11.
Eosin B	33.3	4000	67.	9.8	8.3	4100	6.8	4.9
Uranine	36.4	7000	15.	5.6	5.2	6900	2.7	13.
Iodide	42.8	9000	9.5	5.3	4.8	8400	1.8	24.

Table 2. Results of Toeplitz Analysis

Tracer	x (m)	Channel	$\bar{t}$ (hr)	D (m·mm/hr)	v (mm/hr)	Pe = xv/D	α = D/v (m)
Elbenyl	10.7	1st	2612	8.1	4.7	6.3	1.7
		2nd	14447	0.02	0.74	323	0.03
Eosin Y	24.6	1st	6478	12.4	4.2	8.4	2.9
		2nd	10440	0.2	2.4	314.	0.1
Eosin B	33.3	1st	2814	24.8	12.5	16.8	2.0
		2nd	7198	1.9	4.7	82.6	0.4
		3rd	11980	0.2	2.8	411.	0.1
		4th	16212	0.1	2.1	507.	0.1
Uranine	36.4	1st	3640	5.9	10.2	62.2	0.6
		2nd	6053	1.8	6.1	119.	0.3
Iodide	42.8	1st	7473	9.0	5.9	28.3	1.5
		2nd	14990	6.2	2.9	1980.	0.02

Table 3. Examples of $\bar{b}$ Calculations for Individual Collection Sheets.

Collection Sheet Designation*	Q* ml/hr	Tracers†	$\Sigma v^{\#}$ (mm/hr)	$A=\frac{Q}{\Sigma v}=\bar{b}\omega^{\dagger\dagger}$ (m^2)	$\bar{b}$ (μm)
39+1	0.01	I,EB	18	6×10^{-7}	0.6
39–1	1.7	I,EB	18	9×10^{-5}	90
35+2.5	0.8	I,EB,EY,EL	27	3×10^{-5}	35
33+2.5	6.0	All 5	37.5	1.6×10^{-4}	160
33+0	0.15	I,EB,EY,EL	27	5.6×10^{-6}	7
31+2	5.0	All 5	37.5	1×10^{-4}	130
29+2	1.5	All 5	37.5	4×10^{-5}	40
29+0	25.	All 5	37.5	6.6×10^{-4}	670
27+2	10.	All 5	37.5	2.7×10^{-4}	270
25+0	7.0	All 5	37.5	2×10^{-4}	190

*From Abelin et al. (1987).
†Five tracers are iodine (I), eosin-B (EB), eosin-Y (EY), elbenyl (EL) and Uranin (U).
#From Table 2, first channels; for comparison, the corresponding numbers from Table 1, are Σv (I,EB) = 15 mm/hr; Σv(I+EB+EY+EL) = 22 mm/hr and Σv (all 5) = 28 mm/hr).
††An estimate of $\omega = 1$ m is used.

Table 4. Major Conclusions from Stripa-3D Data (5 Tracers).

Number of Injection Locations	5
Transport Distance (x)	10–43 m
Mean Travel Time ($\bar{t}$)	2200–16000 hours
Peclet Number (all channels)	3.0–400 ($\propto \bar{t}^2$)
Dispersivity α (1st channels)	0.6–2.9 m
Mean Aperture (1st channels)	0.7–670 μm
Aperture Variance, $\sigma/\bar{b}$ (1st channels)	0.35–0.75
Number of Channels seen in 20,000 hours	2–4

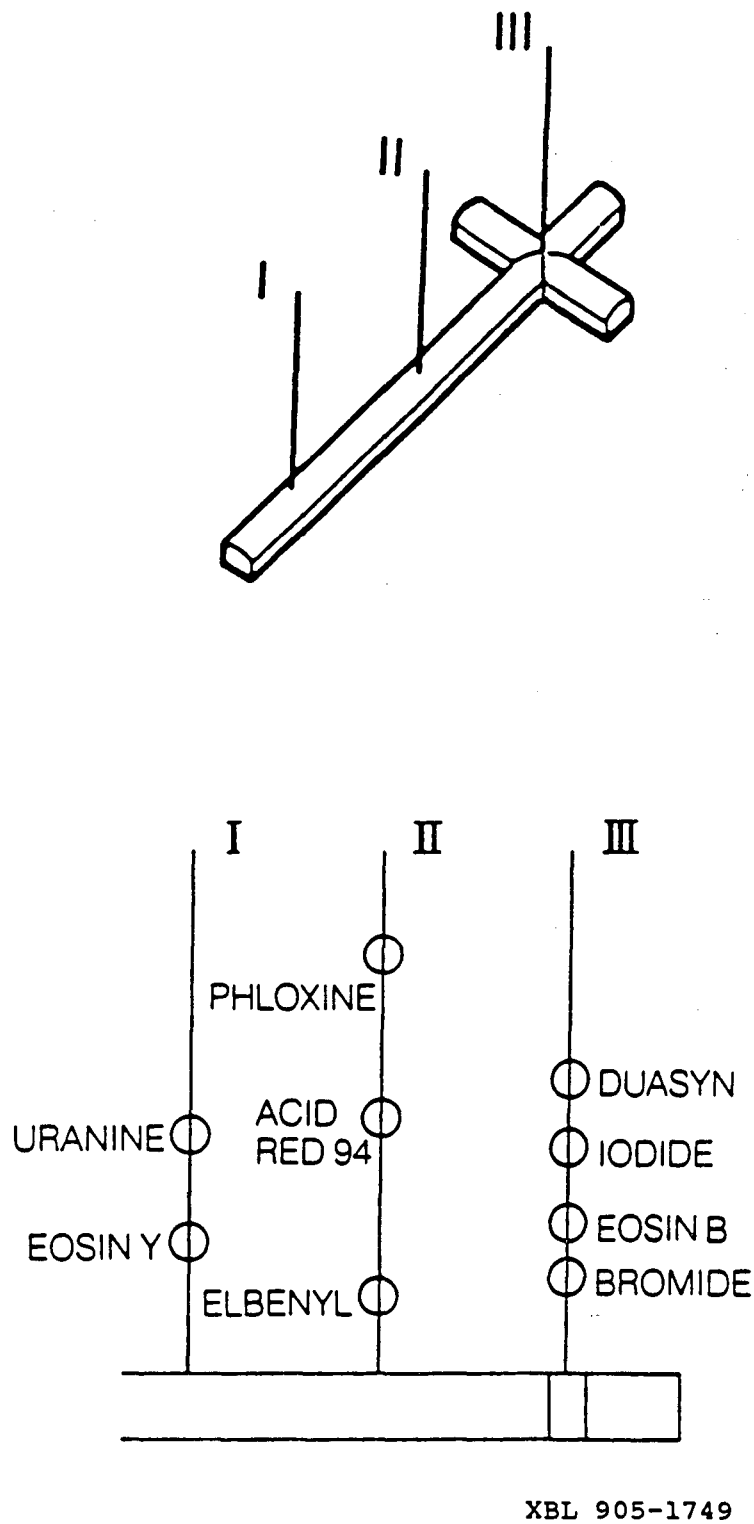

Figure 1. The layout of the Stripa 3D test site with three vertical injection holes is shown above, and the location of tracer injection zones in the three vertical injection holes is shown below

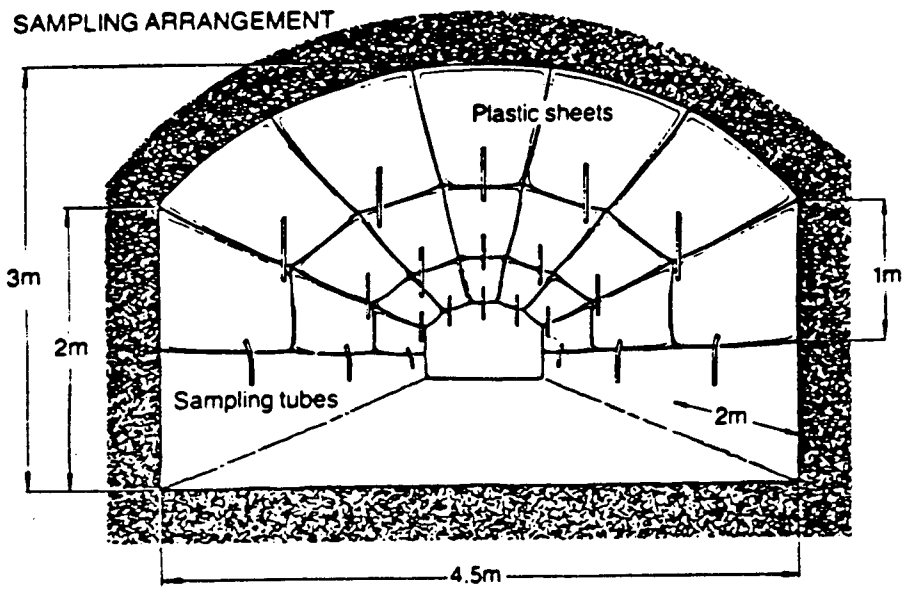

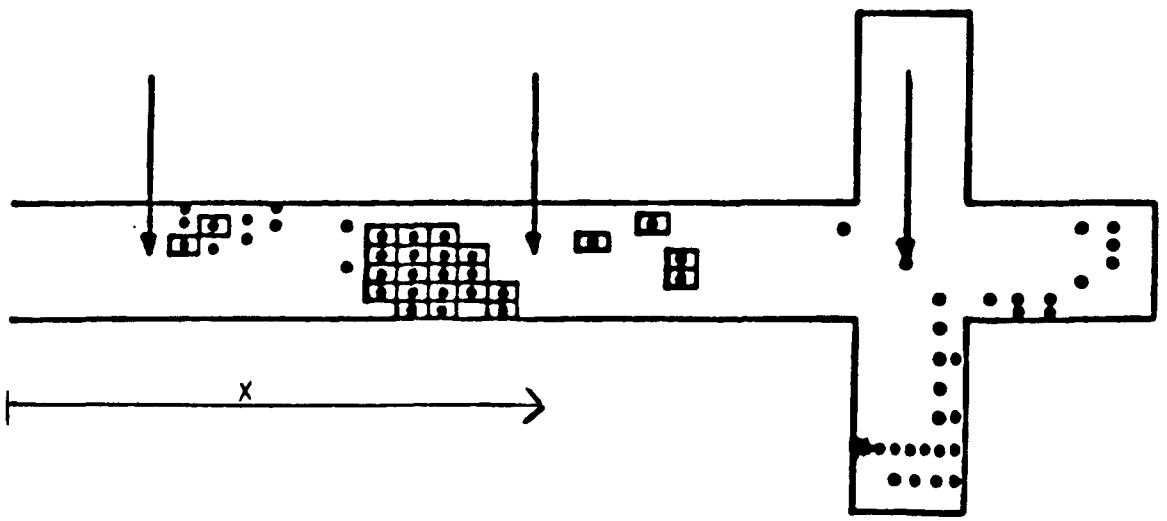

XBL 905-1750

Figure 2. The Stripa 3D sampling arrangement showing placement of plastic sheets for tracer collection is shown above, and a diagram showing tracer distribution in the Stripa 3D test site is shown below. The arrows indicate the positions of the injection holes; dots indicate sheets with significant water flow; and squares indicate sheets where tracers were collected.

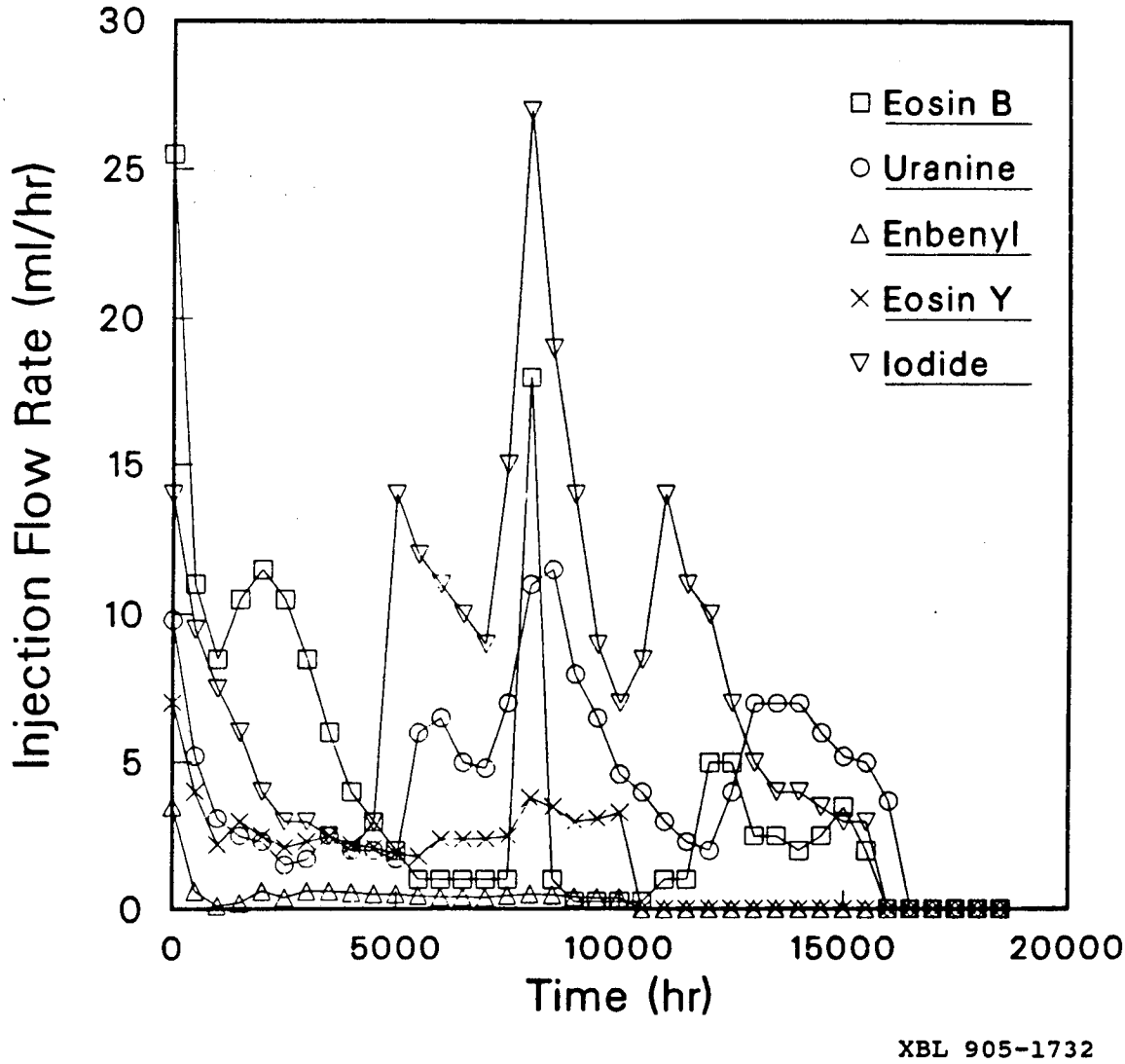

Figure 3. Injection flow rates in ml/hr for the five tracers; points are estimates for average flow rates over 500 hour intervals.

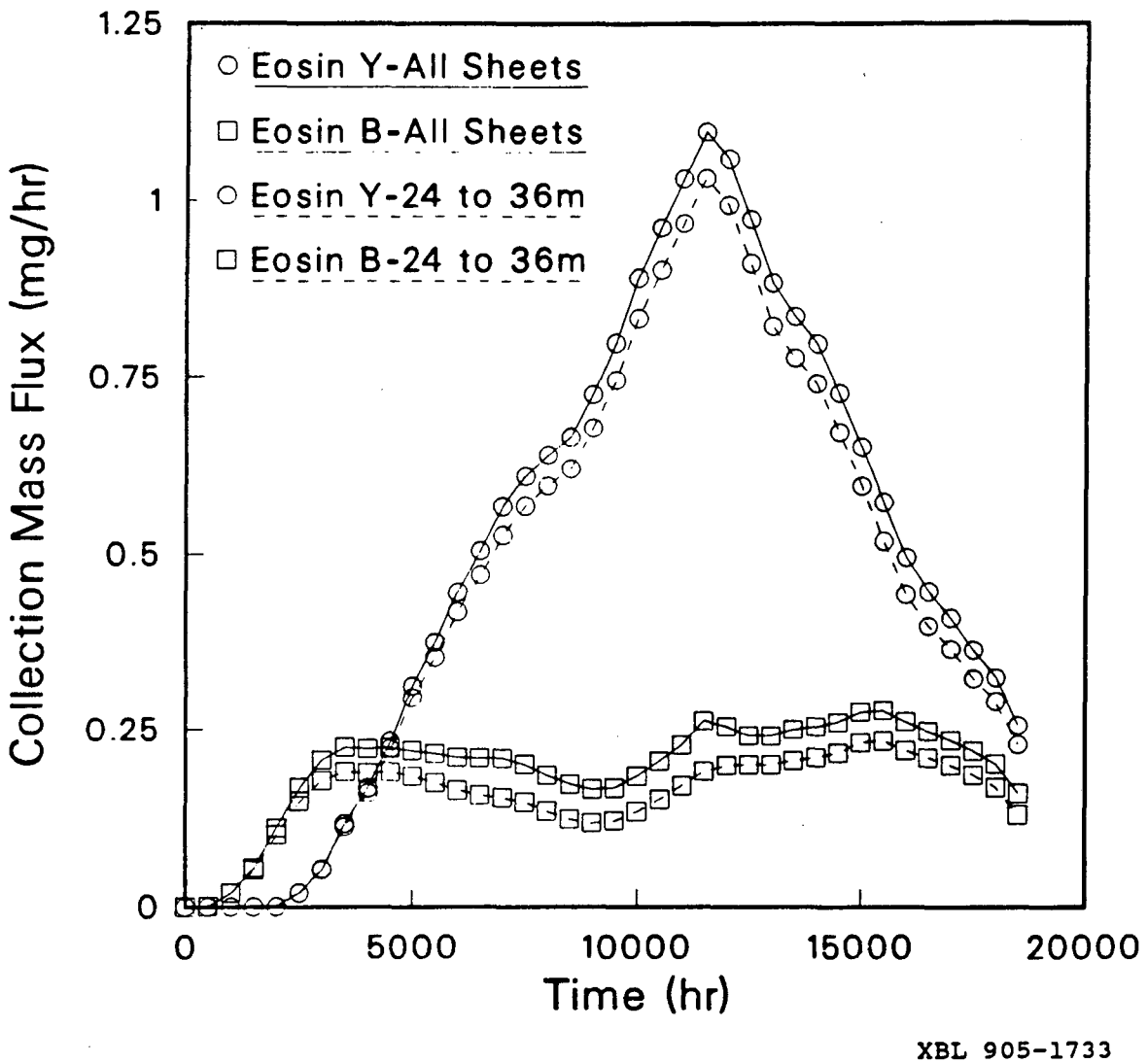

Figure 4a. Mass collection rates for Eosin Y and Eosin B. Note that almost all of the mass is collected in the section from 25 to 36 meters in the tunnel.

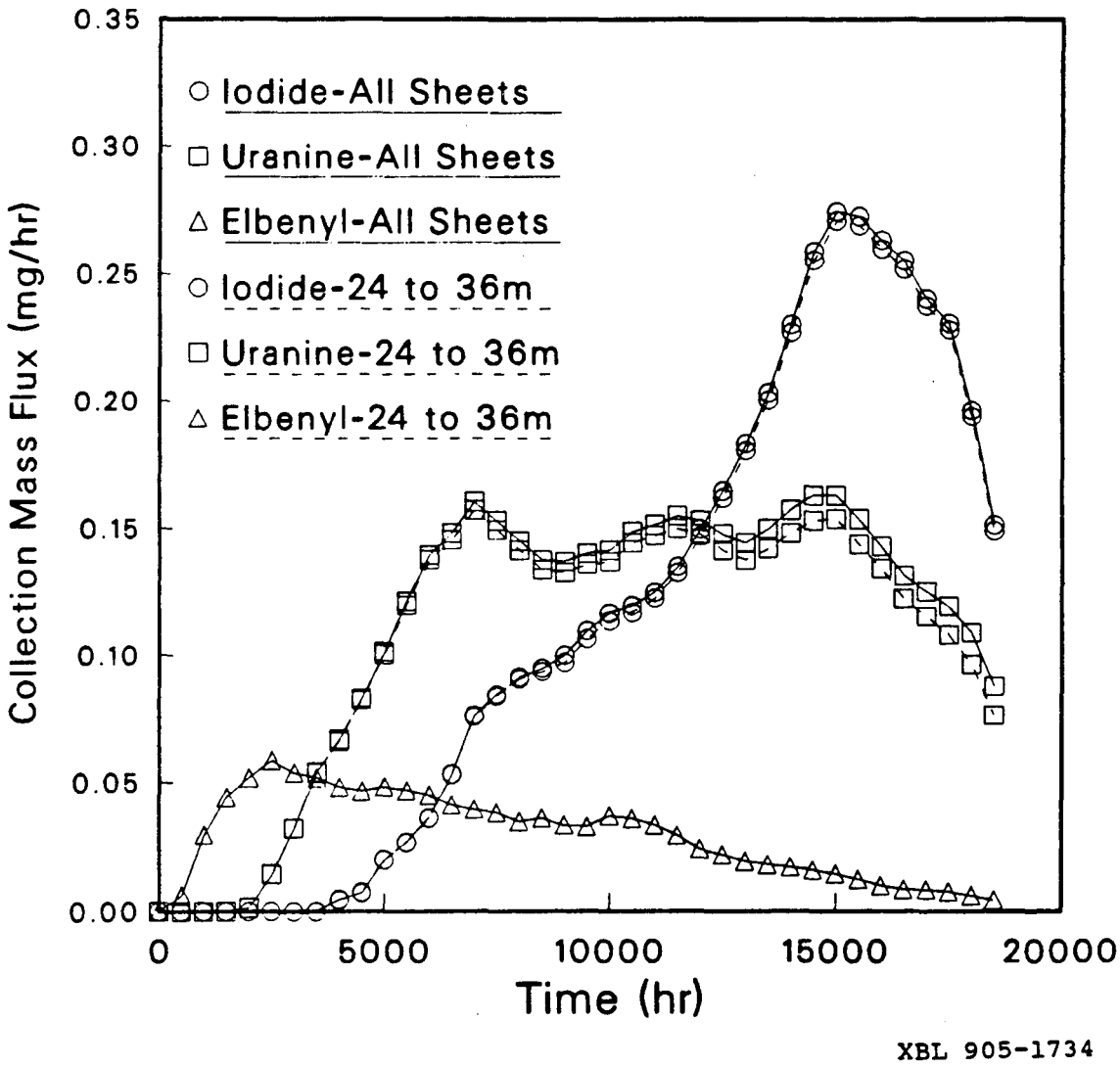

Figure 4b. Mass collection rates for Iodide, Uranine and Elbenyl. Note that almost all of the mass is collected in the section from 25 to 36 meters in the tunnel. In fact, all of the Elbenyl was collected in the section. The vertical scale has been changed by a factor of 3.5 from Figure 4a.

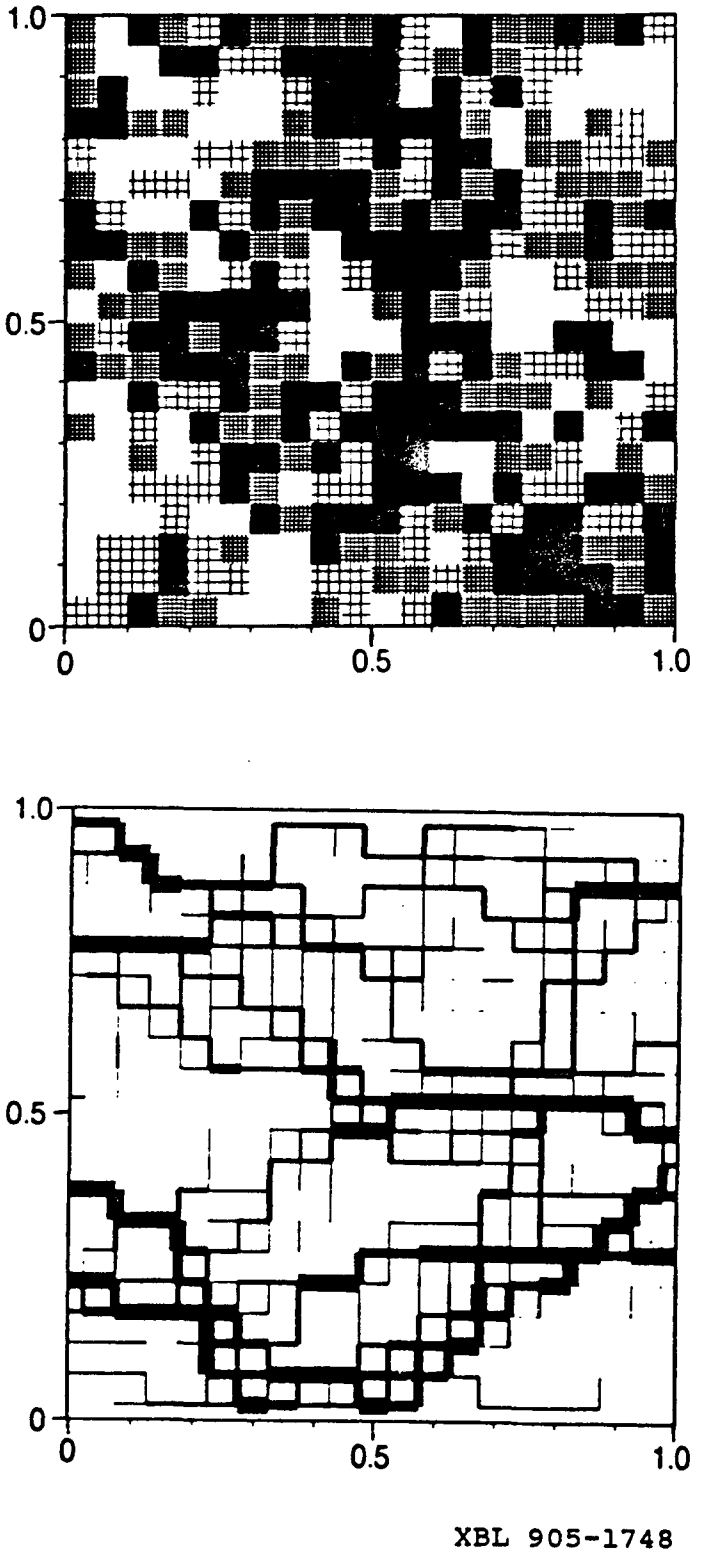

Figure 5. A discretized representation of apertures in a fracture plane is shown above. The magnitudes of the apertures are indicated by shading, with lighter shading corresponding to larger apertures. Relative flow rates for the apertures are shown below, assuming constant pressure boundaries on the left and right, and no flow boundaries for the top and bottom. Thicker lines indicate larger flow rates.

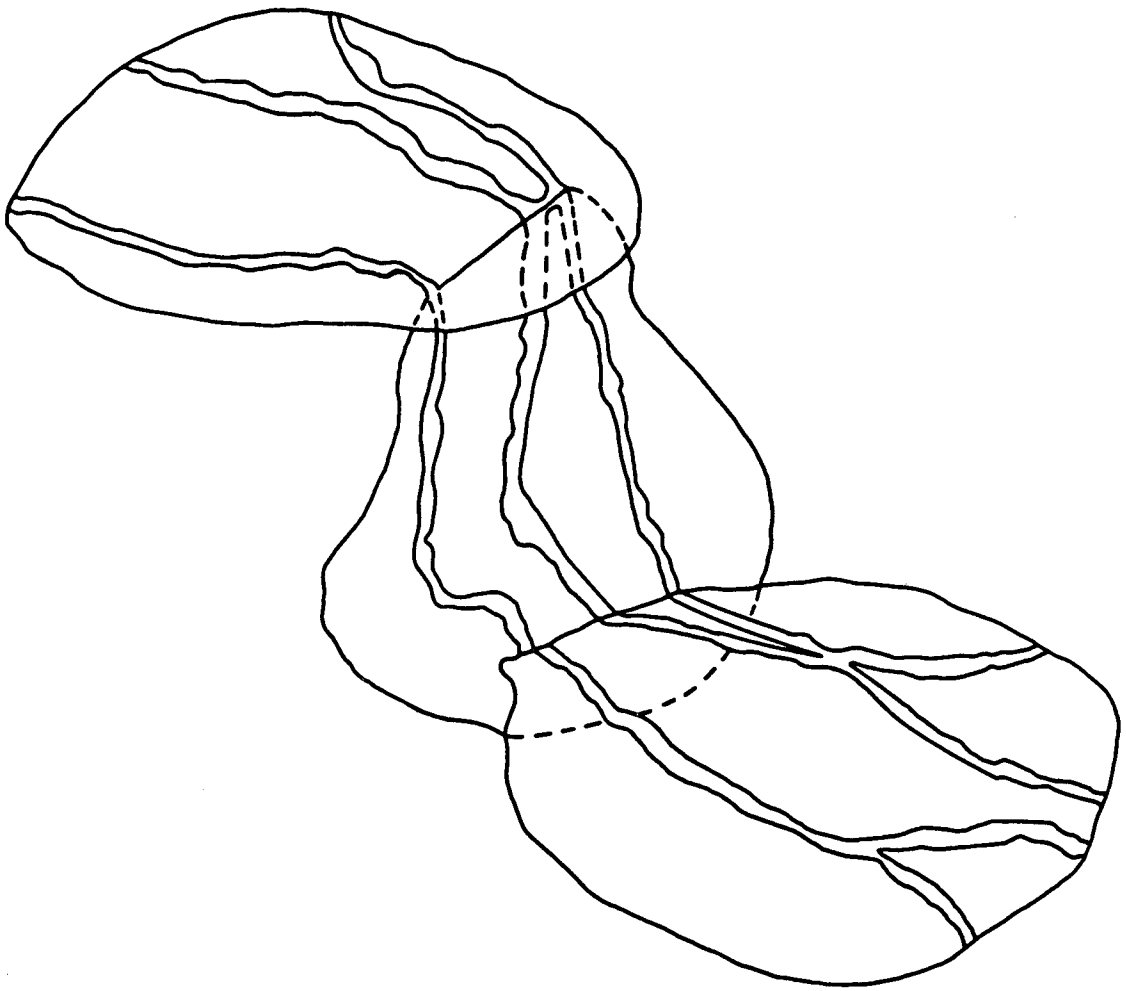

XBL 863-10711

Figure 6. Conceptual model of flow channeling through three fractures in series.

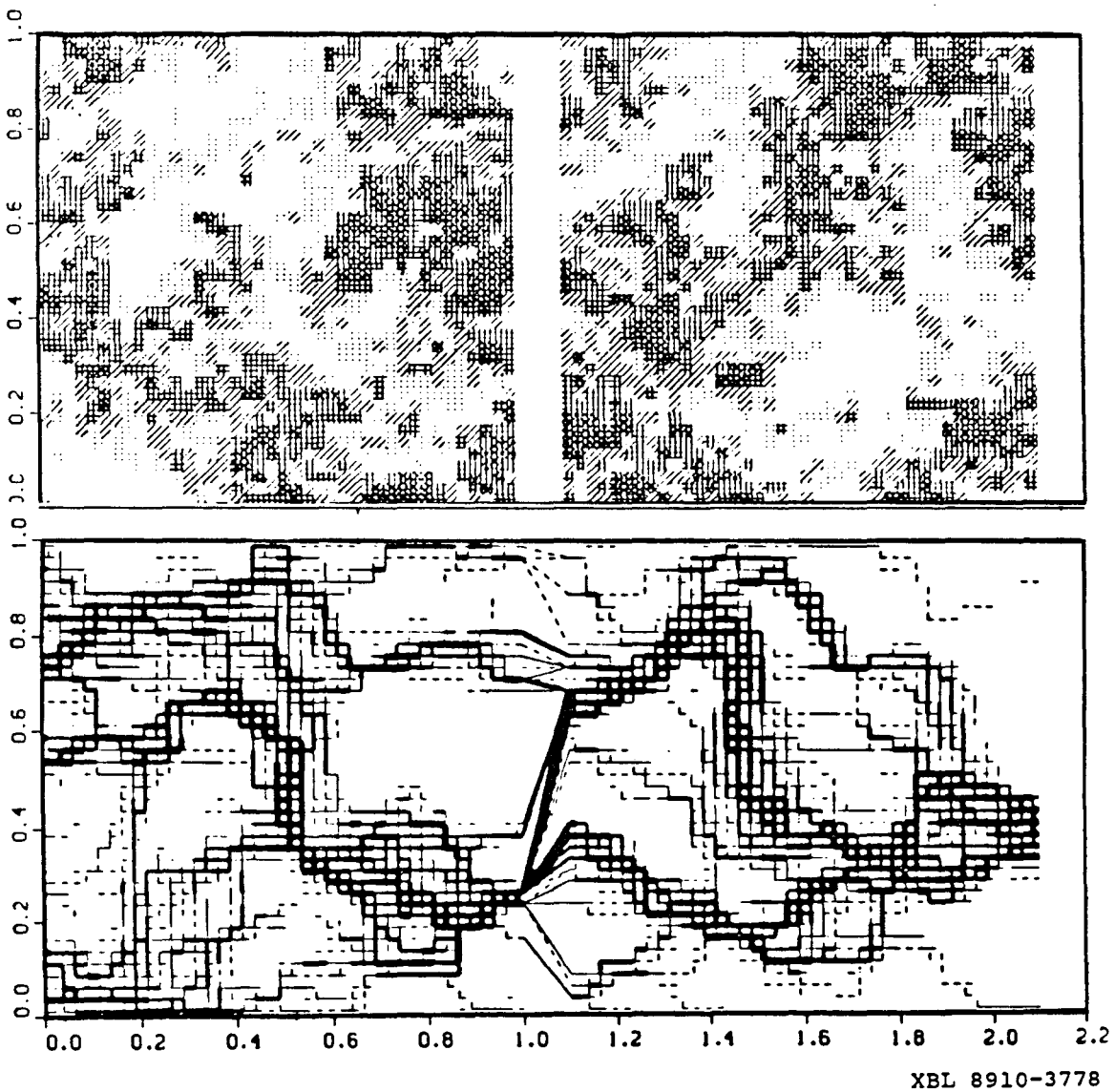

Figure 7. The aperture distribution for the 2D channel model with two connected fractures is shown above. Darker areas have smaller apertures, and lighter areas have larger apertures. The fractures intersect in a line in the center of the figure. Relative flow rates for the apertures are shown below, assuming constant pressure boundaries on the left side of the first fracture and the right side of the second fracture. Flow is from left to right with upper and lower boundaries closed. Thicker lines indicate larger flow rates.

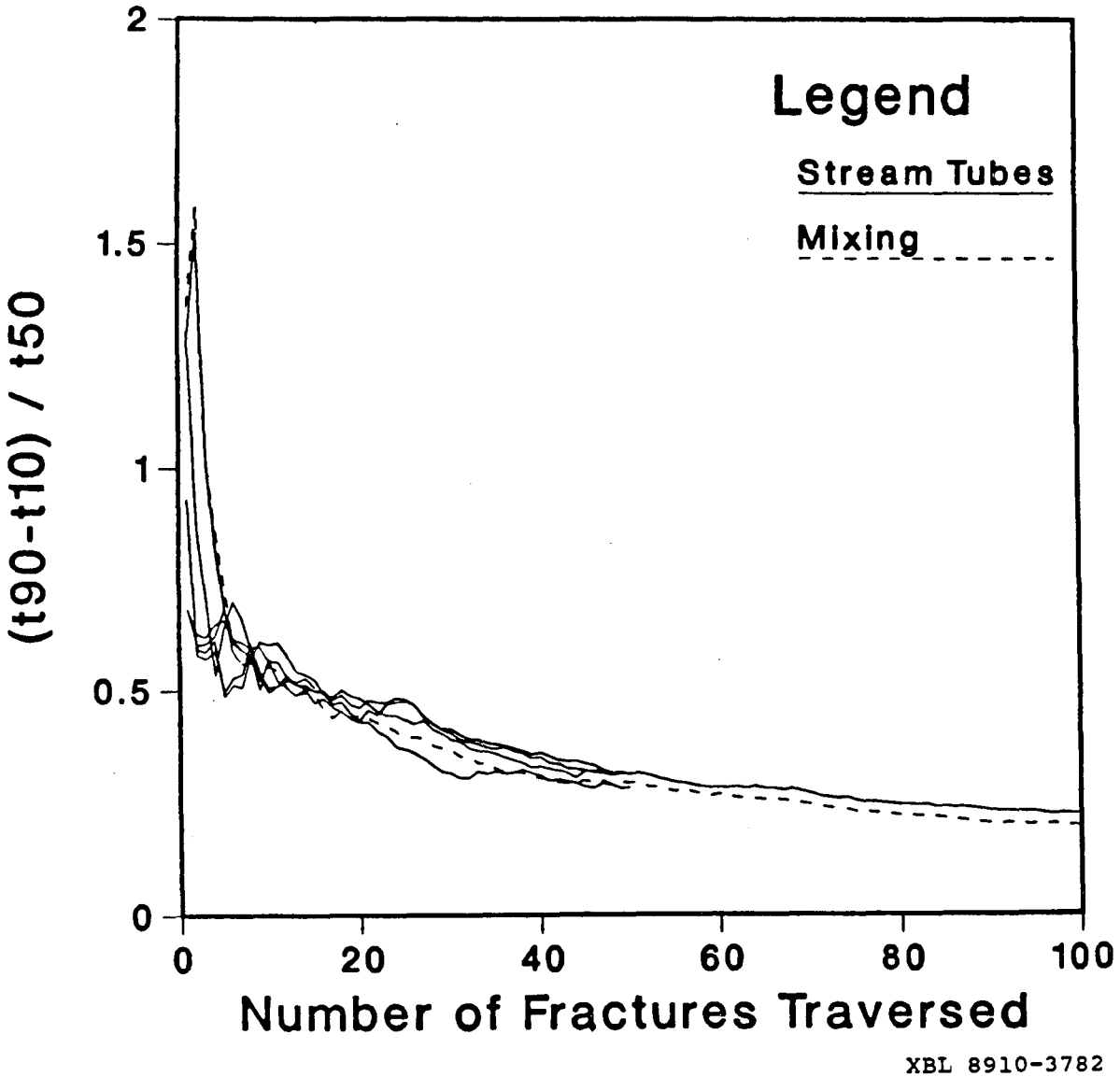

Figure 8. Relationship of measure of dispersion to the number of intersecting fractures traversed. At the intersection two different schemes, total mixing and stream tubes with no mixing, give similar results.

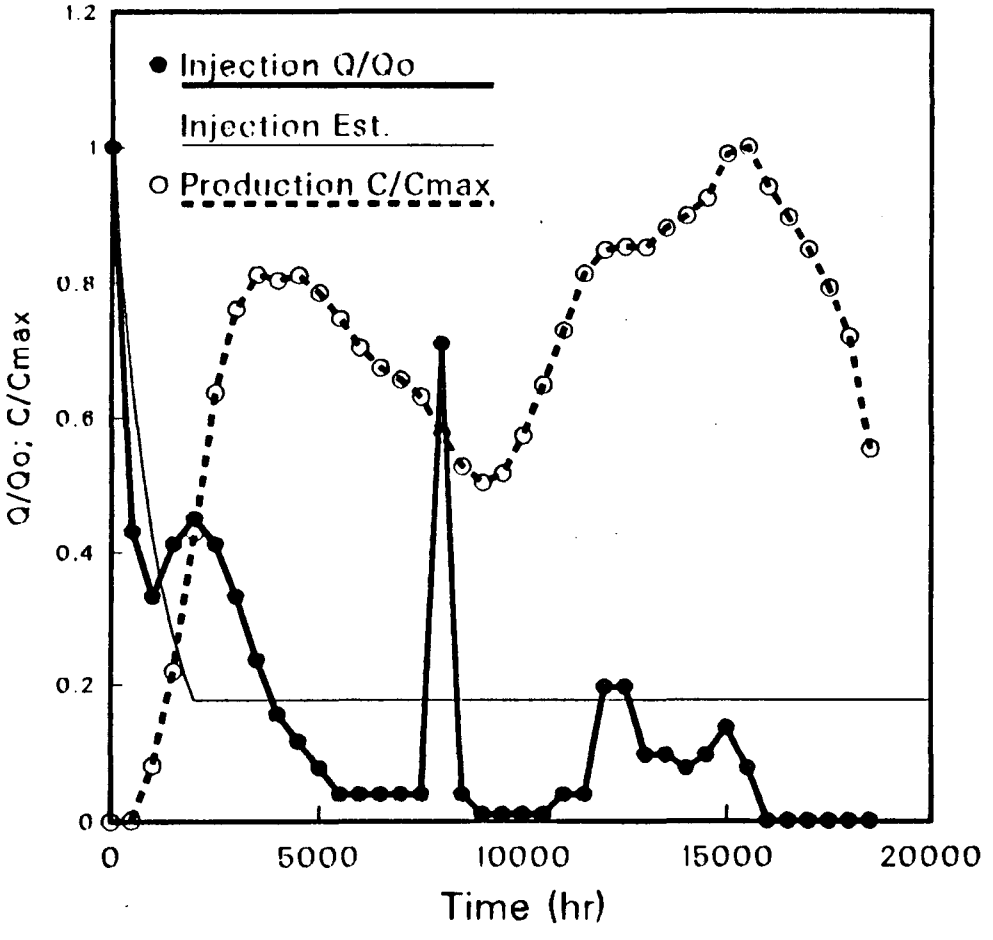

Figure 9. Injection and production data for Eosin B. The injection rates are normalized using the initial injection rate. The collection concentration values are normalized to the maximum concentration at 16,500 hours. The estimate of the injection rate for use with the first peak analysis is based on the injection data up to t_0=2,000 hours, and matches the injection volume up to that time.

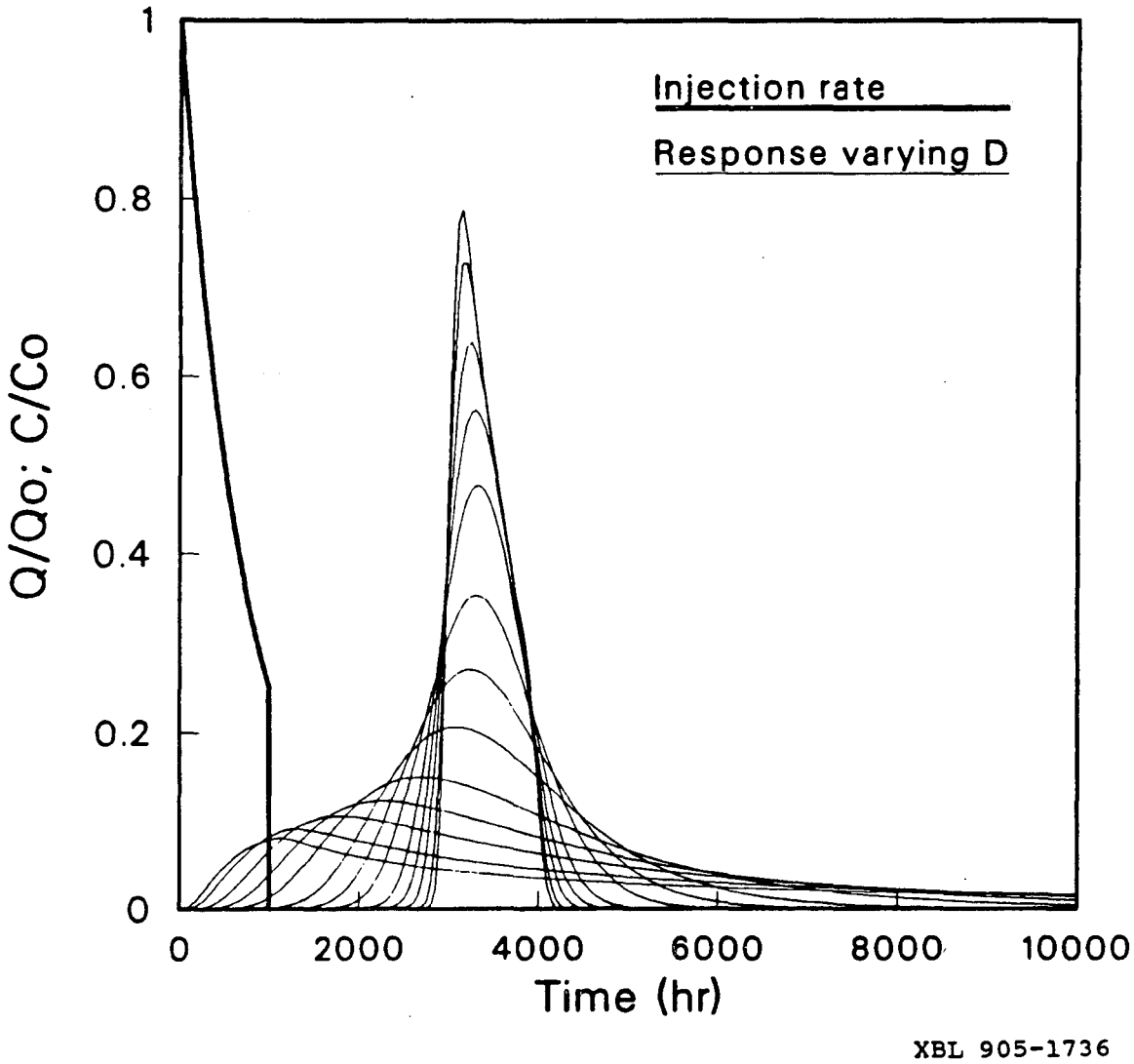

Figure 10. Sensitivity of analytical solution to the dispersion coefficient. The injection rate drops to zero at 1,000 hours. For this particular set of solutions, x=30m, α=1.39×10^{-3}hr^{-1}, v=0.01m/hr, and D ranges from 10^{-4} to 1m^2/hr. Sharper peaks correspond to smaller D values. For D values larger than 0.018m^2/hr, the value of U is imaginary.

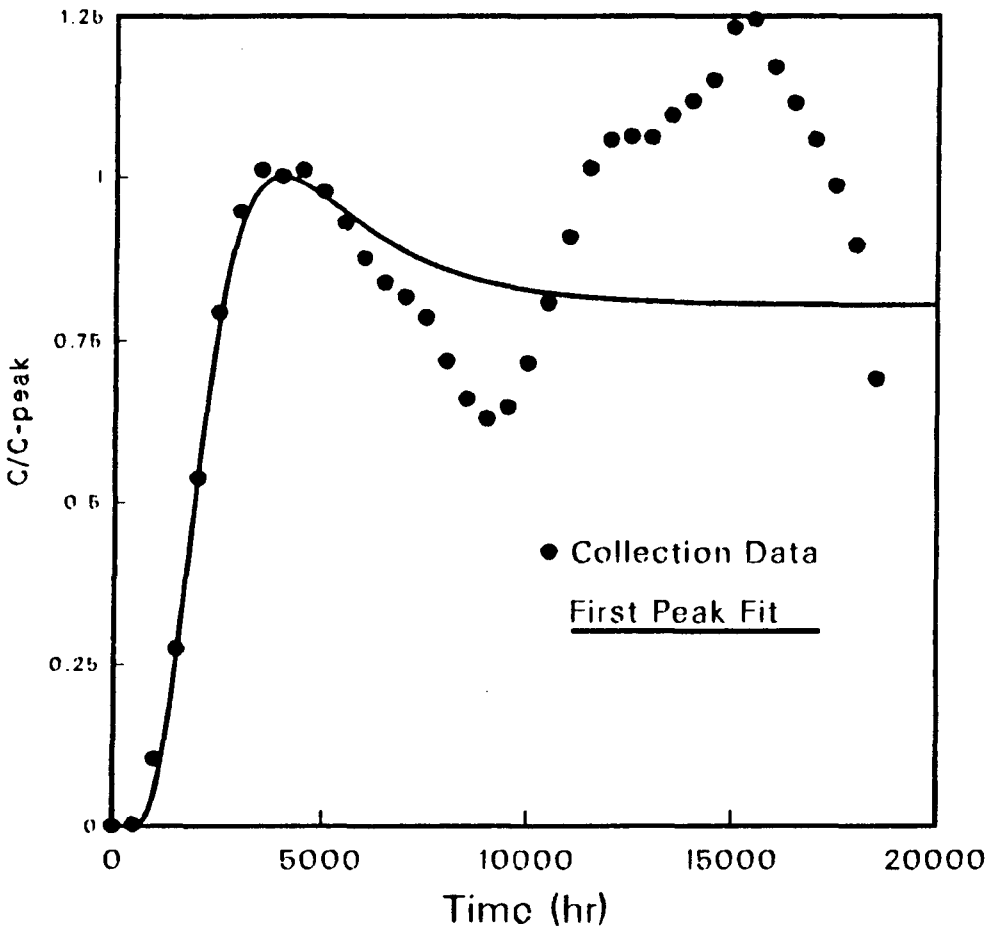

Figure 11. Results of fit to first peak using analytical solution for Eosin B.

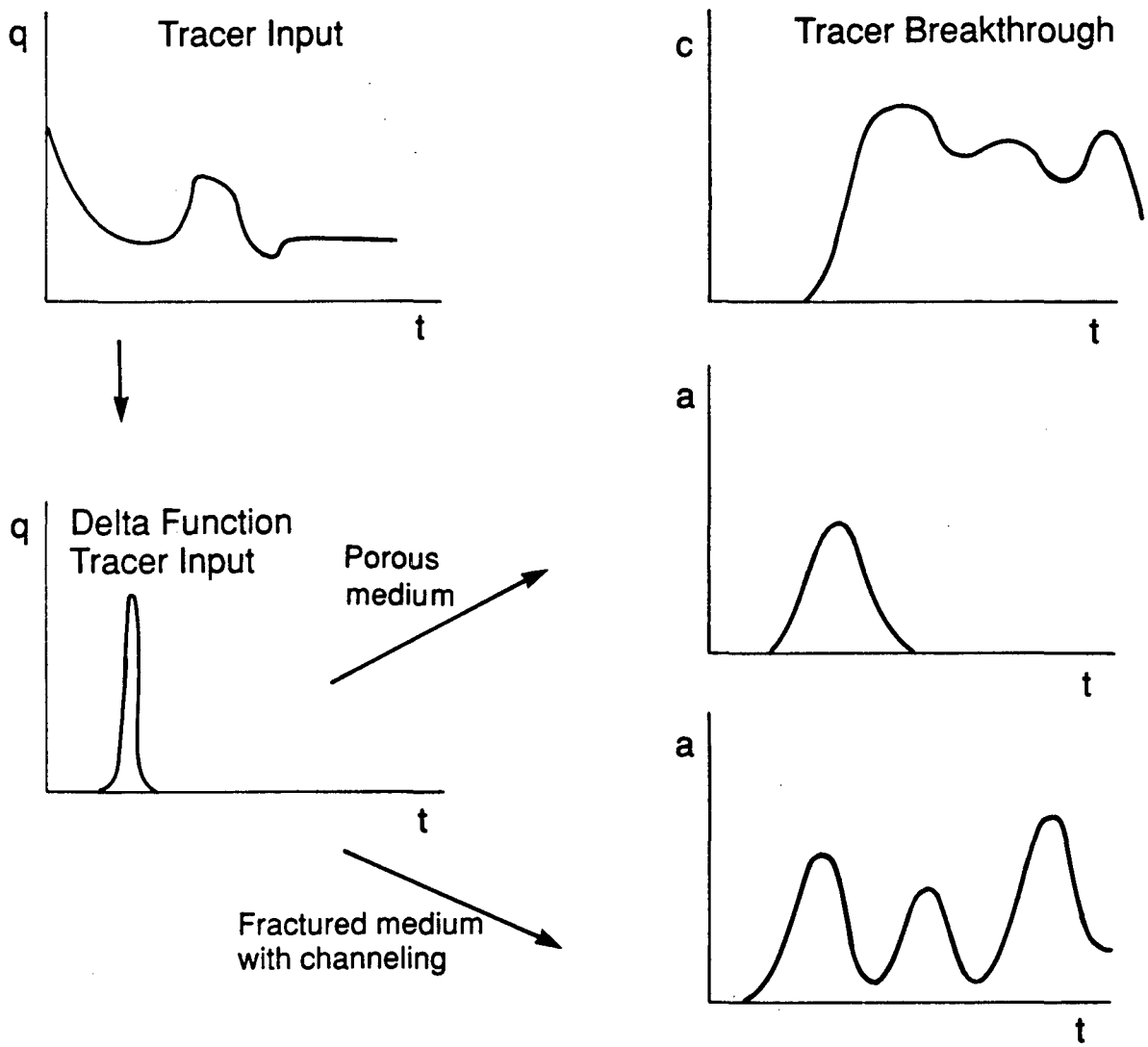

Figure 12. The top two schematic diagrams show the observed tracer injection and breakthrough. The results of deconvolution of the tracer injection data are shown below, as indicated by a pulse tracer injection and the resulting breakthrough curves for a porous medium (single peak) and a fractured medium with channeling (multiple peaks).

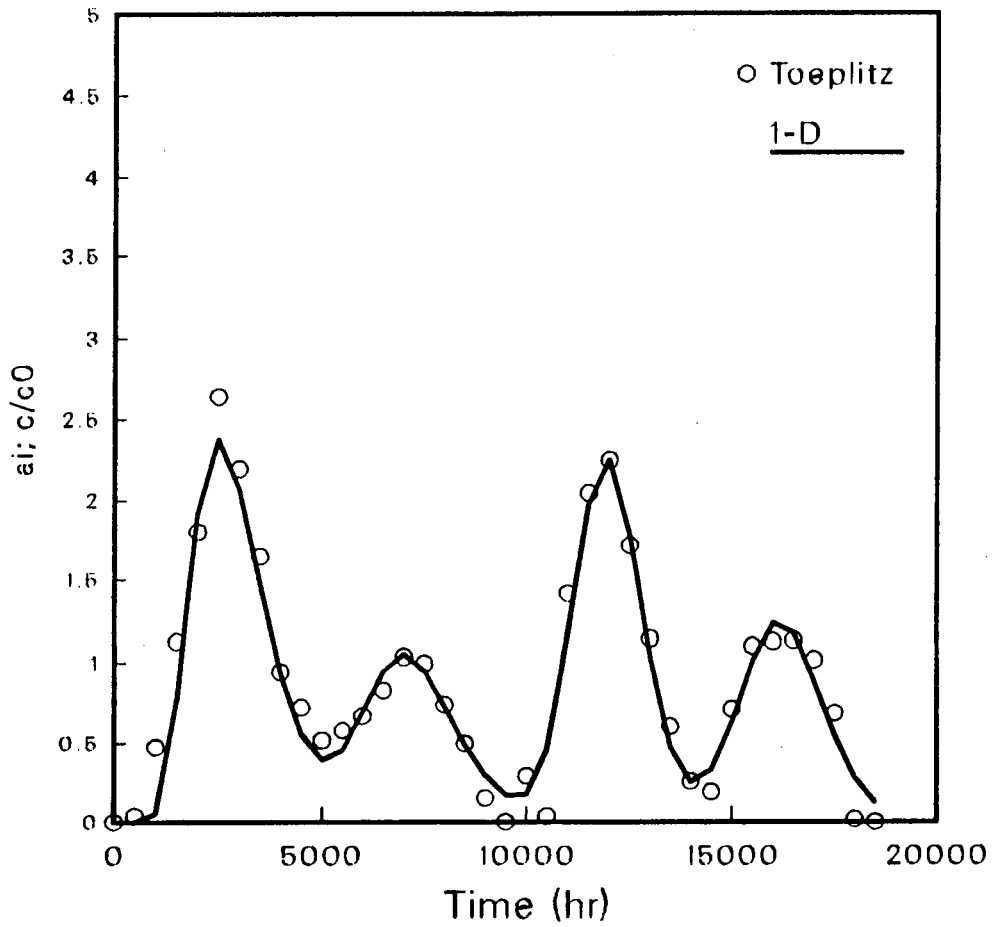

Figure 13. Results of Toeplitz analysis method for Eosin B. The circles are the normalized results of the Toeplitz analysis, and the solid line is the fit of the 1D advection-diffusion equation to the normalized results, separated into distinct peaks.

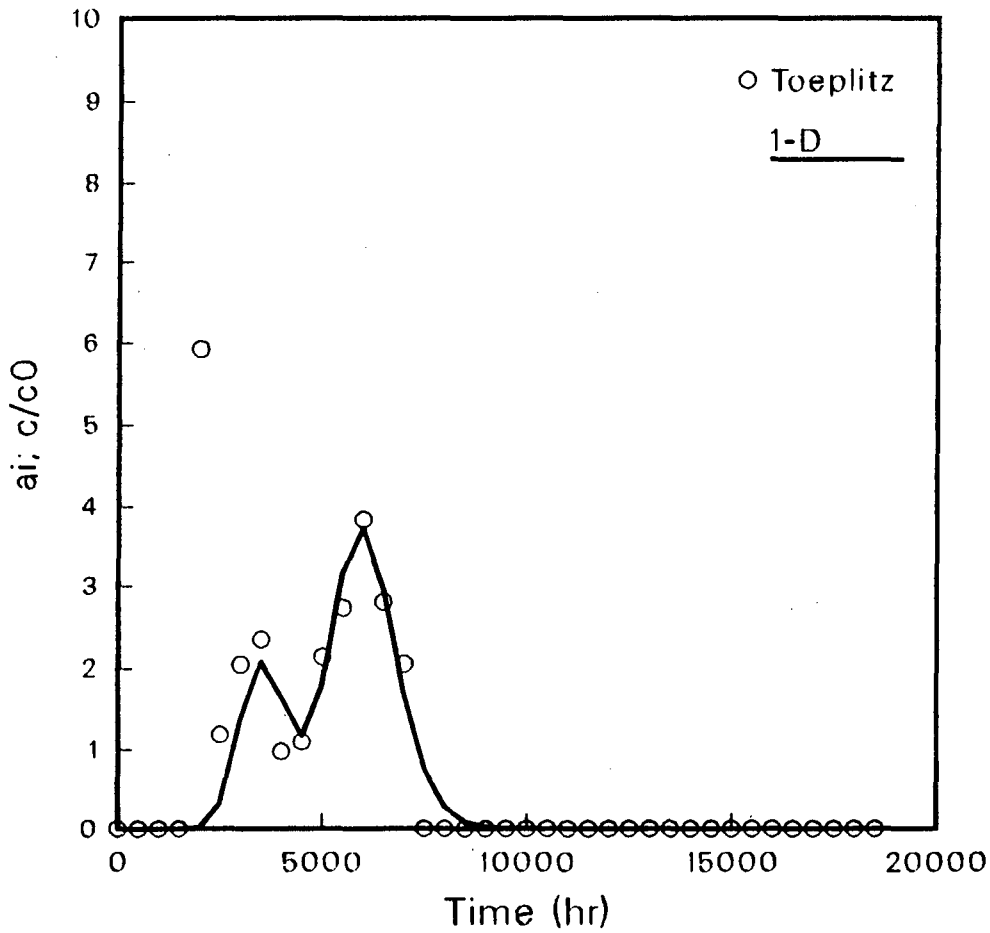

Figure 14. Results of Toeplitz analysis method for Uranine, their fit by equation (9). Note that a Toeplitz solution point at 2,000 hrs is off-scale. This point probably represents an early peak, but there is not sufficient data to determine its characteristics.

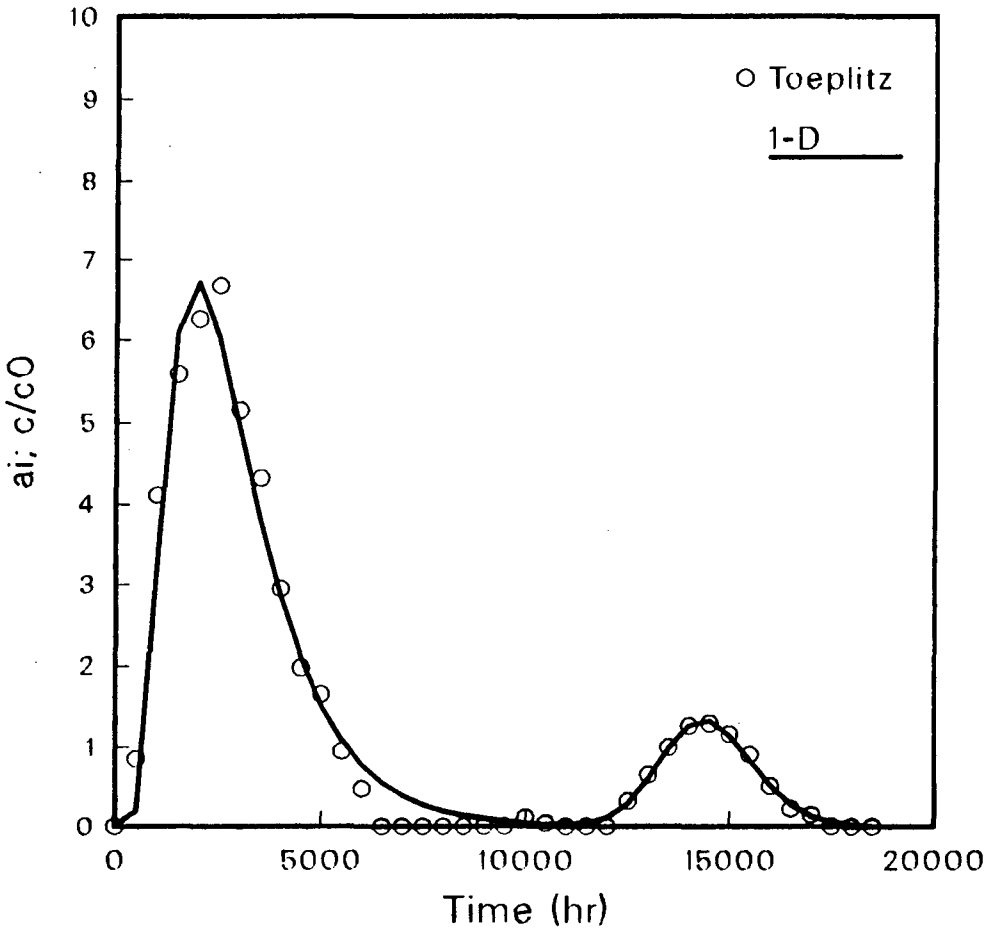

Figure 15. Results of Toeplitz analysis method for Elbenyl, their fit by equation (9).

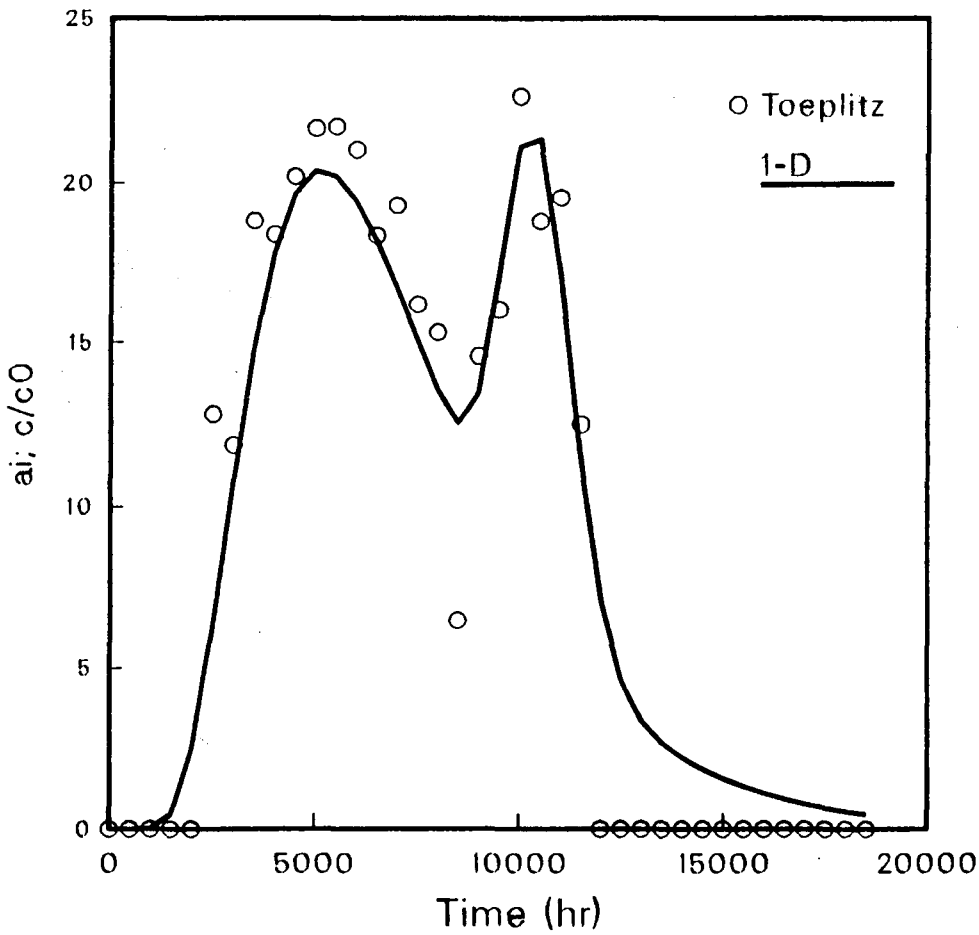

Figure 16. Results of Toeplitz analysis method for Eosin Y, their fit by equation (9).

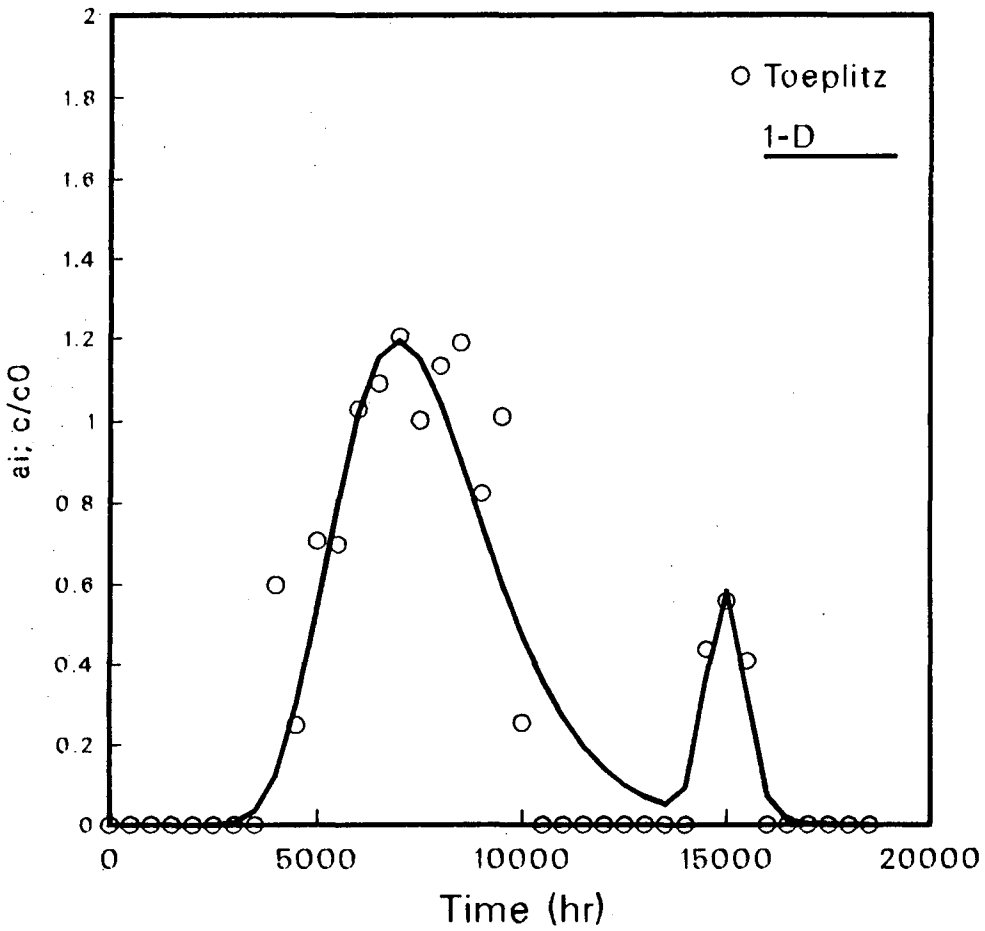

Figure 17. Results of Toeplitz analysis method for Iodide, their fit by equation (9).

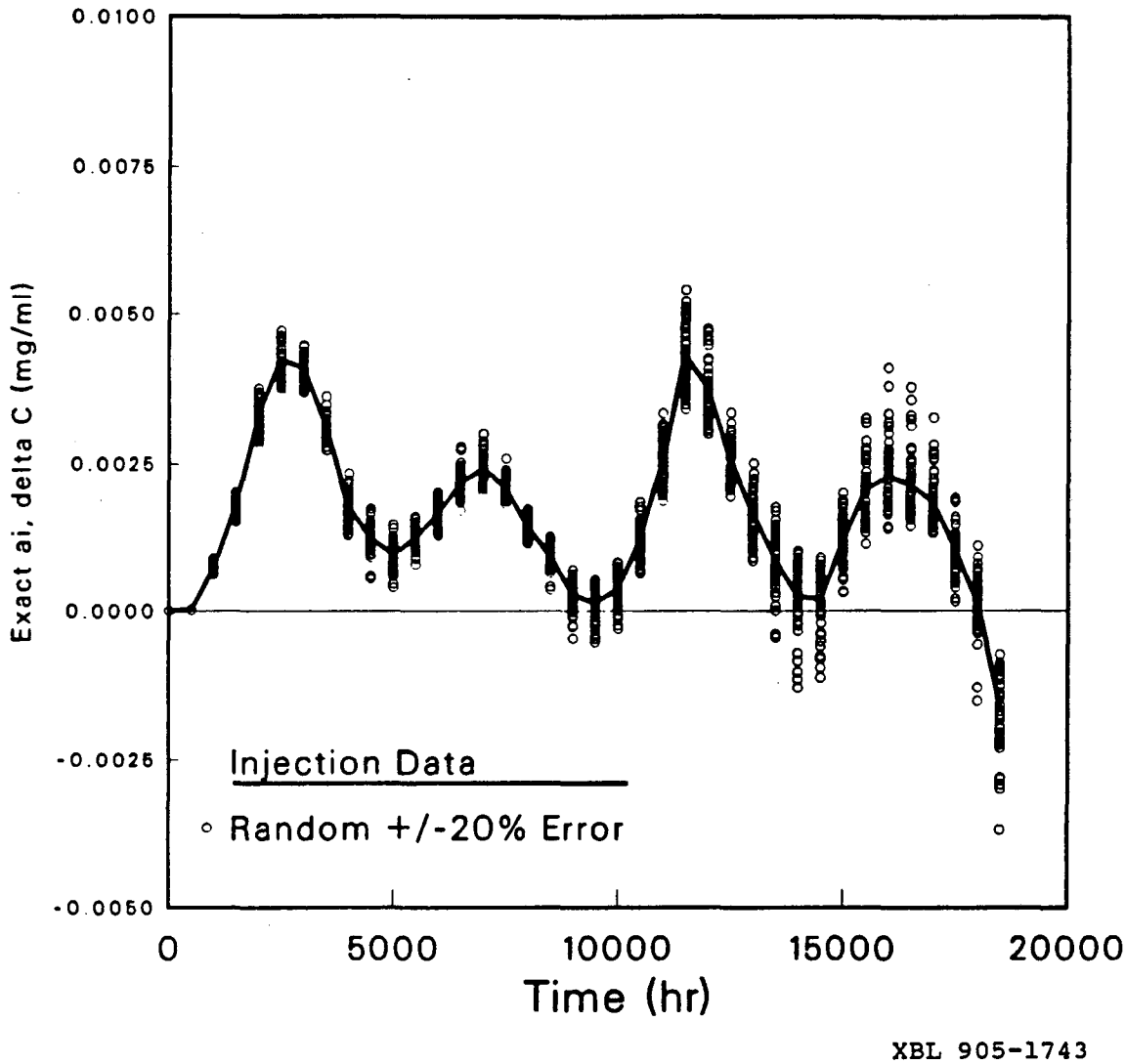

Figure 18. Sensitivity of Toeplitz analysis results to random variability in injection rate data. A random error of ±20% was added to each injection rate for Eosin B, and the effects of fifty sets of random errors on the exact solution are shown here. The solid line shows the exact solution using the original data.

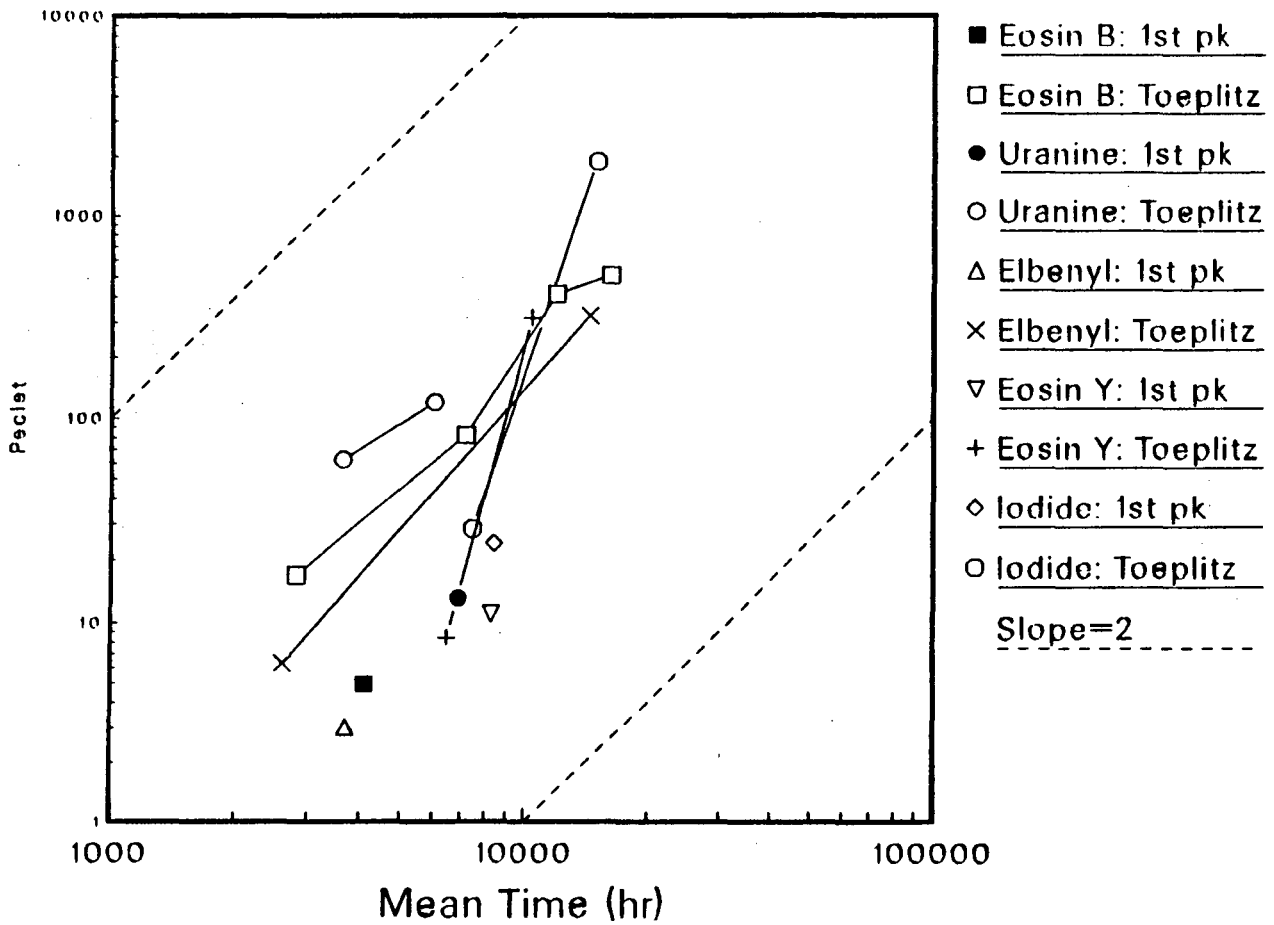

Figure 19. Log-log plot of peclet number versus mean arrival time of each channel. The broken lines indicate a slope of +2.

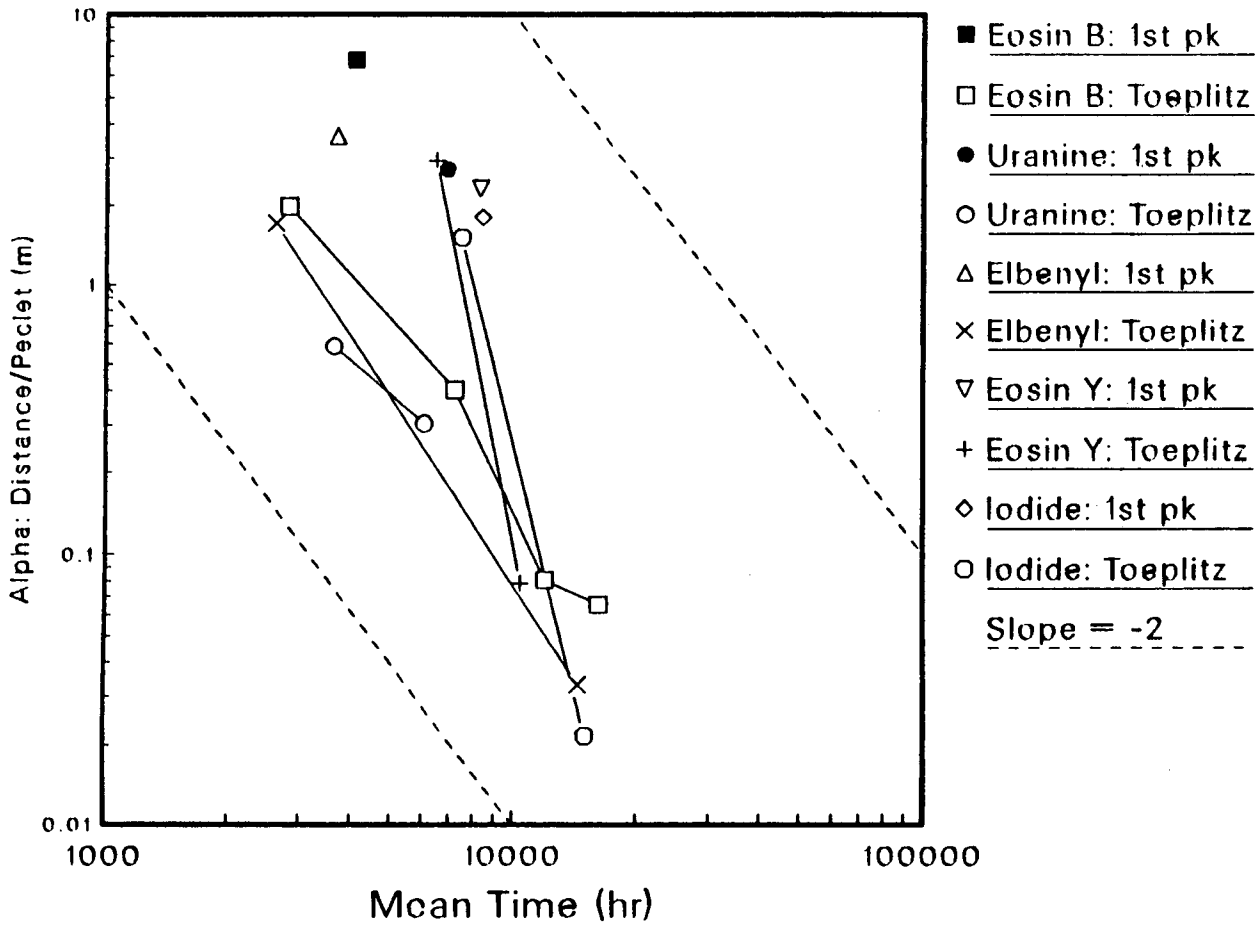

Figure 20. Log-log plot of α=D/v versus mean arrival time of each channel. The broken lines indicate a slope of –2.

LAWRENCE BERKELEY LABORATORY
UNIVERSITY OF CALIFORNIA
INFORMATION RESOURCES DEPARTMENT
BERKELEY, CALIFORNIA 94720